



Charge separation, charge recombination and intersystem crossing in orthogonal naphthalimide–perylene electron donor/acceptor dyad

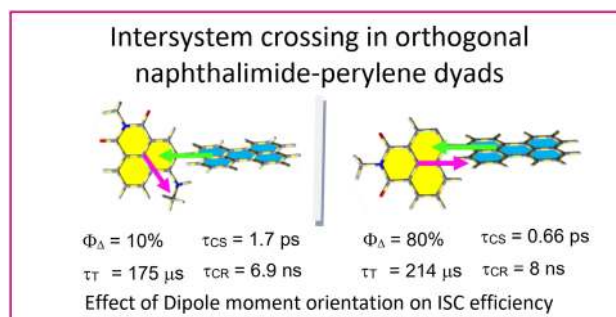
Xi Chen¹ · Junhong Pang² · Muhammad Imran¹ · Xiaolian Li¹ · Jianzhang Zhao^{1,3} · Mingde Li²

Received: 5 October 2020 / Accepted: 25 November 2020 / Published online: 3 January 2021
© European Photochemistry Association, European Society for Photobiology 2021

Abstract

We prepared an orthogonal electron donor/acceptor dyad (NI–Py) with perylene (Py) as electron donor and 4-aminonaphthalimide (NI) as an electron acceptor. The molecule adopts orthogonal geometry due to the steric hindrance exerted by the 4-amino substituents on the NI moiety. The photophysical properties of dyad were studied by steady-state UV–Vis absorption and fluorescence spectroscopies, femtosecond/nanosecond transient absorption spectroscopies and DFT computations. Ground state interaction between the NI and Py units is negligible; however, charge separation occurs upon photoexcitation, indicated by the quenching of the fluorescence of the dyad in polar solvents, i.e. fluorescence quantum yield (Φ_F) is 61.9% in toluene and $\Phi_F = 0.2\%$ in methanol. Spin–orbit-coupled charge transfer-induced intersystem crossing (SOCT-ISC) was confirmed by femtosecond transient absorption spectroscopy (charge separation takes 1.7 ps and charge recombination takes 6.9 ns, in CH_2Cl_2). Nanosecond transient absorption spectra indicated the formation of perylene-localized triplet state, and the triplet state lifetime (175 μs) is much longer than that accessed with the heavy atom effect (3-bromoperylene; 16 μs). The singlet oxygen quantum (Φ_Δ) yield of the dyad is 2.2% in hexane and 9.5% in dichloromethane. The low SOCT-ISC efficiency as compared to the previously reported analogue ($\Phi_\Delta = 80\%$) is attributed to the mismatch of the $^1\text{CT}/T_n$ state energies, and/or the orientation of the NI and Py units, i.e. orthogonal geometry is not sufficient for achieving efficient SOCT-ISC in compact electron donor/acceptor dyads.

Graphical abstract



Supplementary Information The online version contains supplementary material available at <https://doi.org/10.1007/s43630-020-00002-w>.

- ✉ Xiaolian Li
xlianli@dlut.edu.cn
- ✉ Jianzhang Zhao
zhaojzh@dlut.edu.cn
- ✉ Mingde Li
mdli@stu.edu.cn

Extended author information available on the last page of the article

1 Introduction

Triplet photosensitizers (PSs) are molecules which show long-lived triplet state upon photoexcitation, the triplet excited state is populated through intersystem crossing (ISC) [1–3]. The triplet state can phosphorescence, or initiate energy or electron transfer. Triplet PSs have been widely used in photocatalysis, [4–6] photodynamic therapy, [7–10] photovoltaics, [11] and photon upconversion [12–18].

Excellent triplet photosensitizers should show large molar absorption coefficients, high ISC efficiency, and long triplet lifetime [2, 19, 20]. Since the ISC is an electron spin forbidden process, the traditional triplet photosensitizers are mostly based on heavy atom effect, such as those contain Ir(III), Pt(II), Ru(II) and Os(II) transition metal ions [21–26]. However, this type of transitional photosensitizers suffer from some disadvantages, for instance, high cost of preparation, weak absorption of light in the visible region, [27, 28] toxicity and short triplet lifetime (heavy atom effect can enhance the $T_1 \rightarrow S_0$ relaxation) [29, 30]. Thus, it is highly desired to design heavy atom-free triplet PSs. However, it is still a challenge in photochemistry to design heavy atom-free triplet PSs, because the ISC of heavy atom-free organic compounds is elusive and difficult to predict, without the heavy atom effect. There is no general and effective strategy to design heavy atom-free organic compounds showing efficient ISC [2, 31–33].

Charge recombination (CR)-induced ISC has been known for decades in electron donor/acceptor dyads [34–41]. In these dyads, the separation of the electron donor and acceptor is large; as a result, the electronic coupling between the electron donor and acceptor is weak. Thus, the small electron exchange interaction (J values) is small (e.g. $< 0.01 \text{ cm}^{-1}$), the radical pair ISC (RP ISC) may occur, i.e. charge transfer singlet state to charge transfer triplet state ($^1\text{CT} \rightarrow ^3\text{CT}$), [42, 43] then the locally excited triplet state (^3LE) can be populated given the ^3LE energy is lower than ^3CT state. However, the RP ISC kinetics is slow, usually on the ns scale, and fast CR (can be on ps time scale) to ground state (S_0) may reduce the ISC yield [44]. Moreover, these traditional electron donor/acceptor dyads which show RP ISC are difficult to prepare because of the rigid and long linker between the donor and acceptor.

Recently, efficient ISC was observed for compact electron donor/acceptor dyads adopting orthogonal geometry [37–39]. In these *compact* dyads, the linker between the donor and acceptor is short and the synthesis is feasible. The orthogonal orientation of the π -conjugation planes of the donor and acceptor ensure the offsetting of the electron spin angular momentum change of the ISC with the molecular orbital angular momentum change, thus the so-called spin–orbit charge transfer ISC (SOCT-ISC) is fast (on ps time scale) and the ISC can be highly efficient (ISC quantum yield can be 70%) [37–39]. Recently, a variety of visible light absorbing chromophores has been used for the preparation of electron donor/acceptor dyads, for instance, anthracene, [45, 47] Bodipy, [17, 43, 46, 48–50] perylenebisimide, [51] etc. However, it is clear that much room is left for investigation of the SOCT-ISC mechanism. For instances, we used naphthalimide (NI) as electron acceptor and phenothiazine (PTZ) as electron donor, the corresponding electron donor/acceptor dyad showed the

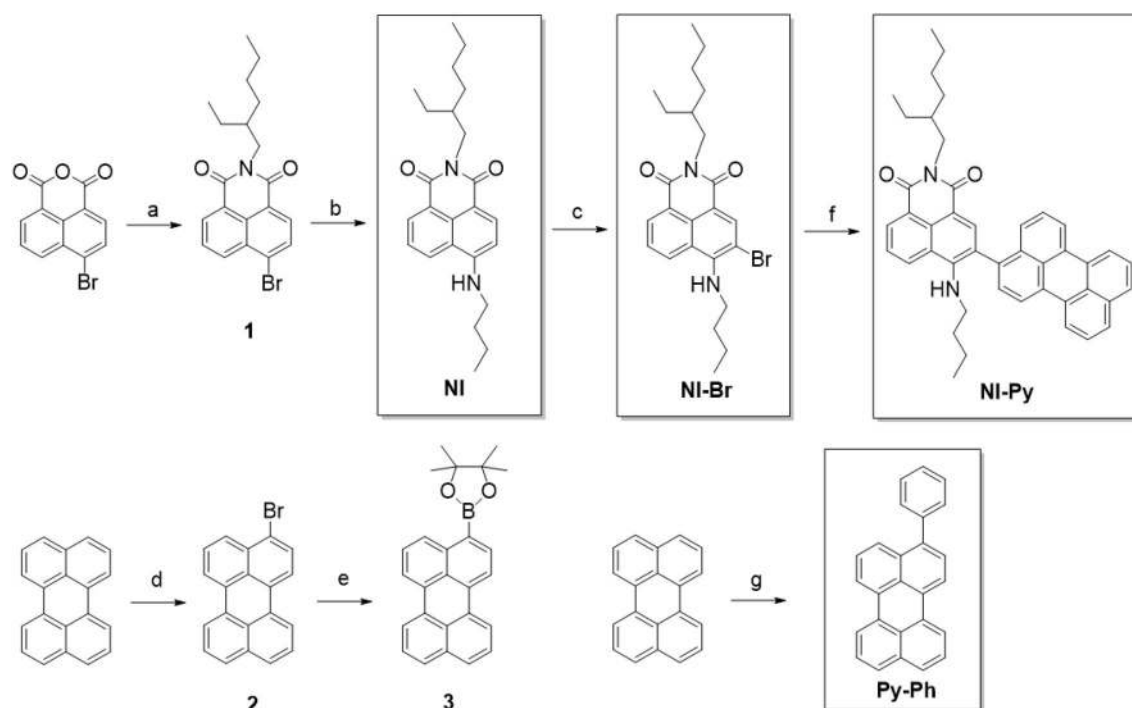
formation of long-lived CT state (most likely ^3CT state) at room temperature (2.6 μs), and thermally activated delayed fluorescence was observed [42]. With perylene (electron donor) attached at the 4-position of NI, efficient SOCT-ISC was observed (singlet oxygen quantum yield $\Phi_\Delta = 80\%$ in dichloromethane) [52]. On the other hand, perylene was also used as an electron acceptor with PTZ as an electron donor, efficient SOCT-ISC was observed (yield $\Phi_\Delta = 60\%$ in dichloromethane) [53]. Our results show that the perylene can be used as either electron *donor* or *acceptor* for dyads showing SOCT-ISC, which is different from the scenario of Bodipy, which is claimed to act only as the electron acceptor in SOCT-ISC systems [49].

To study the molecular diversity of the charge recombination-induced ISC of the compact electron donor/acceptor dyads, herein we attached perylene moiety at the 3-position of NI moiety, and 4-amino substituent was attached at the 4-position of NI to increase the visible light absorption (NI–Py, Scheme 1). The 4-amino NI moiety is an electron acceptor and the perylene unit is the electron donor. Compared to the recently reported NI–perylene dyad without the amino substituent, [52] the current dyad shows different photophysical properties. The photophysical properties were studied with UV–Vis absorption, fluorescence emission, fluorescence lifetime measurements, femtosecond and nanosecond transient absorption spectroscopy, electrochemical characterization, as well as DFT computations. We found the SOCT-ISC efficiency is lower than the recently reported analogue without the amino substituent, and the reason is attributed to the mutual orientation of the NI and the perylene units.

2 Experimental section

2.1 General methods

All raw materials and organic solvents used in the synthesis were used as received, without further purification before use. All organic solvents used in the anhydrous reaction are dried by 4 Å molecular sieves. The inert gas used in the synthesis and spectral measurements is dry N_2 with a purity of 99.999%. Column chromatography uses 200–300 mesh silica gel as the stationary phase. The UV–visible absorption spectrum was tested using a UV2550 dual-beam ultraviolet–visible spectrophotometer (Shimadzu Ltd., Japan). The fluorescence emission and excitation spectra were taken using FS5 fluorescence spectrometer (Edinburgh Instruments, U.K.). Fluorescence lifetime was measured on a OB920 luminescence lifetime spectrometer (Edinburgh Instruments, U.K.). The excitation light source is a picosecond pulsed laser (EPL series).



Scheme 1. Synthesis of **NI-Py** dyad, reagents and conditions: (a) 4-bromo-1,8-naphthalic anhydride, EtOH, reflux 6 h, under N_2 , yield: 72%; (b) butan-1-amine, 2-methoxyethanol, reflux 8 h, under N_2 , yield: 50%; (c) bromine, CH_2Cl_2 , 25 °C, 12 h, under N_2 , yield: 29%; (d) NBS, CCl_4 , 0 °C, 4 h, yield: 84%; (e) bis(pinacolato)diboron,

1,4-dioxane, $Pd(dppf)Cl_2$, CH_2Cl_2 , CH_3COOK , 80 °C, 15 h, yield: 22%; (f) compound **3**, K_2CO_3 , $Pd(pPh_3)_4$, DMF, 80 °C, 4 h, yield: 18%; (g) K_2CO_3 , $Pd(PPh_3)_4$, EtOH/toluene/ H_2O (2:2:1 v/v/v), stirred at 70 °C for 9 h, under N_2 yield: 70%

2.1.1 Synthesis of **1** [54]

Under N_2 atmosphere, the mixture of 4-bromo-1,8-naphthalic anhydride (1 g, 3.63 mmol) and 2-ethyl-1-hexylamine (0.65 mL, 3.986 mmol) in EtOH (100 mL) was refluxed for 6 h at 89 °C. The progress of the reaction was monitored by TLC. After the reaction is complete, the reaction mixture was cooled to room temperature. The solvent was removed under reduced pressure, then the crude product was purified by column chromatography (silica gel; hexane/dichloromethane 3:1, v/v). A yellow solid was obtained (1.02 g, yield 72%). 1H NMR ($CDCl_3$, 400 MHz): δ 8.67 (d, 1H, $J=8.07$ Hz), 8.59 (d, 1H, $J=8.56$ Hz), 8.47 (d, 1H, $J=7.83$ Hz), 8.06 (d, 1H, $J=7.95$ Hz), 7.87–7.83 (m, 1H), 4.17–4.06 (m, 2H), 1.98–1.89 (m, 1H), 1.41–1.26 (m, 8H), 0.95–0.86 (m, 6H). MALDI-TOF-HRMS: calc ($[C_{20}H_{22}NO_2Br]^+$), $m/z=387.0834$; found, $m/z=387.0844$.

2.1.2 Synthesis of **NI** [55]

Under N_2 atmosphere, compound **1** (400 mg, 1.032 mmol) and *n*-butylamine (377.64 mg, 0.512 mmol) were dissolved in 2-methoxyethanol (10 mL), then the mixture was refluxed for 8 h. After the reaction is complete, water (50 mL) was added and the mixture was extracted with dichloromethane

(3 \times 25 mL). The organic layer was dried over anhydrous Na_2SO_4 . The solvent was removed under reduced pressure. The residue was purified by column chromatography (silica gel, CH_2Cl_2 / Petroleum ether = 1:1, v/v). A yellow solid was obtained (0.98 g, yield 50%). 1H NMR ($CDCl_3$, 400 MHz), δ 8.59 (d, $J=7.3$ Hz, 1 H), 8.48 (d, $J=8.3$ Hz, 1 H), 8.10 (d, $J=7.7$ Hz, 1 H), 7.64 (t, $J=7.8$ Hz, 1 H), 6.75 (s, 1 H), 4.15–4.06 (m, 2 H), 3.43 (t, $J=7.2$ Hz, 2 H), 1.96–1.93 (m, 1 H), 1.84–1.77 (m, 2 H), 1.58–1.49 (m, 2 H), 1.41–1.29 (m, 9 H), 1.04 (t, $J=7.3$ Hz, 3 H), 0.94–0.85 (m, 6 H). MALDI-TOF-HRMS: calc ($[C_{20}H_{22}NO_2Br]^+$), $m/z=380.2464$; found, $m/z=380.2468$.

2.1.3 Synthesis of **NI-Br** [55]

At room temperature, Br_2 (2 mL, 0.50 g, 3.2 mmol) was mixed with anhydrous CH_2Cl_2 (20 mL), then the solution was added dropwise to a solution of **NI** (0.40 g, 1 mmol) in CH_2Cl_2 (20 mL). Under N_2 atmosphere, the reaction mixture was stirred for 12 h. After the reaction was completed, the solvent was removed under reduced pressure, and the residue was purified by column chromatography (silica gel, CH_2Cl_2 ; petroleum ether = 1:1) to obtain **NI-Br** as a yellow solid (0.30 g, yield 29%). 1H NMR ($CDCl_3$, 400 MHz): δ 8.64 (s, 1H), 8.59 (d, $J=7.5$ Hz, 1 H), 8.47 (d, $J=8.4$ Hz,

1 H), 7.65 (t, $J=7.9$ Hz, 1 H), 4.18–3.95 (m, 2 H), 3.67 (t, $J=7.0$ Hz, 2 H), 1.94–1.91 (m, 1 H), 1.76–1.70 (m, 2 H), 1.50–1.43 (m, 2 H), 1.41–1.19 (m, 9 H), 1.02–0.81 (m, 9 H). MALDI–TOF–HRMS: calc ($[\text{C}_{20}\text{H}_{22}\text{NO}_2\text{Br}]^+$), $m/z=458.1569$; found, $m/z=458.1561$.

2.1.4 Synthesis of 2 [56]

Under N_2 atmosphere, *N*-bromosuccinimide (NBS, 70.5 mg, 1.0 mmol) was dissolved in anhydrous THF (5 mL) and the solution was added to a solution of perylene (100 mg, 1.0 mmol) in anhydrous THF (5 mL). The mixture was stirred in an ice-water bath for 4 h. After the reaction was completed, the mixture was poured into water (30 mL) and extracted with CCl_4 (30 mL). The organic layer was dried over anhydrous MgSO_4 . The solvent was removed under reduced pressure to obtain compound **2** as a yellow solid (0.128 g, yield 84%). ^1H NMR (CDCl_3 , 400 MHz): δ 8.21–8.05 (m, 4H), 7.95 (d, $J=8.1$ Hz, 1H), 7.74–7.65 (m, 3H), 7.57–7.44 (m, 3H). MALDI–TOF–HRMS: calc ($[\text{C}_{20}\text{H}_{22}\text{NO}_2\text{Br}]^+$), $m/z=330.0044$; found, $m/z=330.0052$.

2.1.5 Synthesis of 3 [57]

Under N_2 atmosphere, KOH (10 mg, 0.18 mmol) was added into the dry 1,4-dioxane (25 mL), then the mixture was stirred for 15 min. Took the supernatant (15 mL), bis(pinacolato)diboron (114.39 mg, 0.45 mmol), CH_3COOK (88.182 mg, 0.9 mmol), and 3-bromoperylene (100 mg, 0.3 mmol) were added. The mixture was then bubbled with N_2 for 20 min. Then $\text{Pb}(\text{dppf})\text{Cl}_2$ (10 mg, 0.01 mmol) was added, and the mixture was stirred at 80 °C for 15 h. The reaction mixture was cooled to room temperature, water (5 mL) and dichloromethane (20 mL) for extraction, then the organic layer was washed with brine for three times. After the organic liquid was dried over Na_2SO_4 , the solvent was removed under reduced pressure. The compound was separated through a silica gel column to obtain a yellow solid (silica gel, CH_2Cl_2 : petroleum ether = 2:3) 0.025 g, yield 22%. ^1H NMR (CDCl_3 , 400 MHz): δ 8.76–8.65 (d, 1H, $J=8.29$ Hz), 8.25–8.17 (m, 4H), 8.07–8.05 (d, 1H, $J=7.53$ Hz), 7.71–7.67 (m, 2H), 7.56–7.47 (m, 3H), 1.44 (s, 12H), 1.33 (s, 1H), 1.28 (m, 14H), 1.25 (s, 4H), 0.88–0.86 (s, 6H), 0.07 (s, 2H). MALDI–TOF–HRMS: calc ($[\text{C}_{20}\text{H}_{22}\text{NO}_2\text{Br}]^+$), $m/z=378.1791$; found, $m/z=378.1795$.

2.1.6 Synthesis of NI–Py [58]

Compound **3** (100 mg, 0.26 mmol), **NI–Br** (121 mg, 0.26 mmol), and K_2CO_3 (109 mg, 0.79 mmol) were mixed in dry DMF (10 mL), then water (0.1 mL) was added. After bubbling of the mixture with N_2 for 15 min, $\text{Pd}(\text{PPh}_3)_4$ (15.3 mg, 1.325 mmol) was added. Then the mixture was

stirred at 80 °C for 4 h under N_2 atmosphere. After the reaction was completed, the reaction mixture was cooled to room temperature. The mixture was extracted with dichloromethane, then washed with water (4×50 mL), and dried with Na_2SO_4 . The solvent was removed under reduced pressure and the crude product was purified by column chromatography (silica gel, CH_2Cl_2 : Hexane = 2:3, v/v) to give yellow solid (30 mg, yield 18%). Mp (174.4–176.5 °C). ^1H NMR (CDCl_3 , 400 MHz): δ 8.67 (d, $J=7.2$ Hz, 1 H), 8.60 (d, $J=8.8$ Hz, 1 H), 8.50 (s, 1 H), 8.35–8.23 (m, 4 H), 7.82–7.72 (m, 3 H), 7.59–7.49 (m, 3 H), 7.48–7.42 (m, 1 H), 7.40–7.34 (m, 1 H), 4.21–4.04 (m, 2 H), 3.28 (s, 2 H), 1.48–1.24 (m, 12 H), 1.07–1.84 (m, 9 H), 0.64 (t, $J=7.3$ Hz, 3 H). ^{13}C NMR (CDCl_3 , 125 MHz): δ 167.73, 165.01, 164.38, 35.81, 134.72, 133.28, 131.30, 128.21, 127.29, 126.71, 120.66, 120.11, 65.58, 53.42, 44.04, 37.99, 31.94, 30.82, 29.70, 28.79, 24.10, 23.12, 22.70, 19.66, 19.19, 14.14, 13.50, 10.72. MALDI–TOF–HRMS: calc ($[\text{C}_{20}\text{H}_{22}\text{NO}_2\text{Br}]^+$), $m/z=629.3168$; found, $m/z=629.3160$.

2.2 Measurement of singlet oxygen quantum yields

1,3-Diphenylisobenzofuran (DPBF) was used as a $^1\text{O}_2$ scavenger to determine the singlet oxygen quantum yield (Φ_Δ) by monitoring the absorbance of DPBF at 414 nm.

$$\Phi_{\text{sam}} = \Phi_{\text{std}} \left(\frac{1 - 10^{-A_{\text{std}}}}{1 - 10^{-A_{\text{sam}}}} \right) \left(\frac{I_{\text{sam}}}{I_{\text{std}}} \right) \left(\frac{\eta_{\text{sam}}}{\eta_{\text{std}}} \right)^2 \quad (1)$$

In the above formula, Φ represents the singlet oxygen quantum yield; A represents the absorbance at the excitation wavelength (usually in the range 0.2 ~ 0.3); I represents the slope of the plot of absorption of DPBF against the photoirradiation time; η represents the refractive index of the solution; Sam represents the sample to be tested; std represents the standard sample [59].

2.3 Nanosecond transient absorption spectroscopy

The nanosecond transient absorption spectrum was obtained by a LP980 nanosecond laser flash photolysis spectrometer (Edinburgh Instruments, U.K.), the pulsed light source was a wavelength tunable nanosecond laser (oscilloscope HE 355 LD UV). A Tektronix TDS 3012C oscilloscope was used for digitizing the signal. The data was analyzed with L900 software. The sample solution was purged with N_2 for 15 min before measurements. To eliminate the triplet–triplet–annihilation quenching effect, a kinetic model with TTA effect considered was used for the simulation [60].

2.4 Femtosecond transient absorption spectra

The fs-TA measurements were performed based on a femtosecond TI: Sapphire regenerative amplified TI: Sapphire laser system (Coherent, Astrella-Tunable-F-1k) and femtosecond transient absorption spectrometer system (Ultrafast Systems, Helios Fire). The repetition frequency of amplifier is 1 kHz and the pulse width of 800 nm is 84 fs, the output power of 800 nm from amplifier is 7.2 W. The probe pulse was obtained using approximately 4% of the amplified 800 nm output from the Astrella to generate a white-light continuum (320–700 nm) using a CaF₂ plate. The probe beam was split into two beams before passing through the sample. One probe beam travel through the sample, and the other is sent directly to the reference spectrometer that monitors the fluctuations in the probe beam intensity.

Fiber optics was coupled to a multichannel spectrometer with a CMOS sensor that had a 1.5 nm intrinsic resolution. The maximum extent of the temporal delay was 8000 ps. The instrument response function was determined to be ca. 120 fs. At each temporal delay, data were averaged for 2 s and collected by the acquisition system. For the experiments described in this study, the sample solution was excited by a 400-nm pump beam (from TOPAS). The sample solutions were excited in a 2-mm path-length cuvette. The absorption intensity at 400 nm of sample is ca. 0.7 when UV–Vis absorption spectra were measured in a 2-mm path-length cuvette. The data were stored as three-dimensional (3D) wavelength–time–absorbance matrices that were exported for use with the fitting software. Chirp correction was done for the all the data shown here. The attenuation of transient species adopts a sequential model and is obtained by global fitting [61].

2.5 DFT calculation

Density functional theory (DFT) was used to optimize the ground state geometry of the molecules, and time-dependent density functional theory (TD-DFT) was used to calculate the excited state energy. The calculations were performed with Gaussian 09 software and at the B3LYP/6-31G(d) level [62].

3 Results and discussion

3.1 Design and synthesis of the compounds

With 4-amino substituent attached on NI moiety, the absorption is red-shifted as compared to the unsubstituted NI. Thus we selected the 4-aminoNI as one of the chromophore. Previously it was reported that the 4-aminoNI is with reduction potential of -2.04 V (vs. Fc/Fc⁺), as comparison

to the -1.88 V (vs. Fc/Fc⁺) of unsubstituted NI [63]. On the contrary, the perylene moiety is with oxidation potential of $+0.55$ V (vs. Fc/Fc⁺) [53]. Thus, we suppose the NI moiety is the electron acceptor, and the perylene unit is the electron donor. The connection of the perylene unit is at the 3-position of NI moiety, i.e. the ortho-position of the 4-amino substituted NI, thus significant steric hindrance is expected, and the dyad may adopt orthogonal geometry, which is beneficial to the SOCT-ISC [45, 46, 64].

The synthesis is with 4-bromonaphthalimide as the starting material, compound **1** was prepared by refluxing 4-bromoNI with 2-ethylhexylamine. Then by reaction with 1-butylamine, the intermediate NI was obtained. Bromination of NI gives intermediate NI-Br in 29% yield. 1-Peryleneboronic acid ester was used for the Pd(0)-catalyzed Suzuki–Miyaura coupling reaction to give the final product NI-Py in 18% yield. Py-Ph and NI were used as reference compounds in the study. The molecular structures of all the compounds were characterized with ¹H NMR and HR MS spectra.

3.2 UV–Vis absorption spectra

The UV–Vis absorption spectra of the compounds were studied (Fig. 1). For dyad NI-Py, a broad, structured absorption band was observed in the range of 350 nm–500 nm (Fig. 1a). The spectrum is almost the sum of the mixed solution of compounds NI and Py-Ph, thus the electronic interaction between the NI and the perylene units in the dyad is negligible at ground state (S₀) [65–67]. This is attributed to the orthogonal geometry and thus the inhibition of the π -conjugation (see later section). This orthogonal geometry excluded the formation of CT absorption bands in the UV–Vis absorption spectrum [68–70]. The absorption spectra of the four compounds were compared (Fig. 1b), it was found that the NI unit and the perylene unit absorption bands are in the same range, but a structureless band was observed for the NI unit, and absorption band with

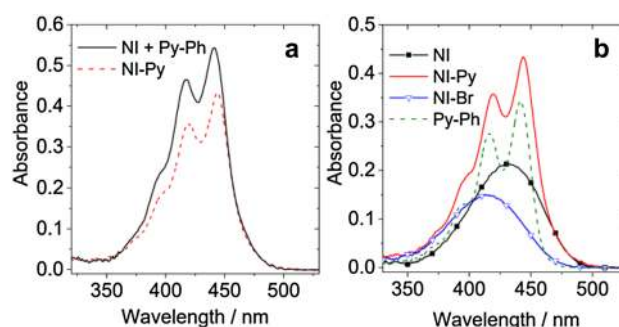


Fig. 1 a UV–Vis absorption spectra of NI-Py and NI+Py-Ph, b UV–Vis absorption spectra of NI, NI-Br, NI-Py, Py-Ph in acetonitrile. $c = 1.0 \times 10^{-5}$ M, 20 °C

significant vibrational progression was observed for the perylene unit.

3.3 Fluorescence spectroscopy

The fluorescence of the compounds was compared in different solvents (Fig. 2). In *n*-hexane, **Py-Ph** gives a strong emission band in the range of 450–600 nm, with vibrational progression feature. For compounds **NI** and **NI-Br**; however, broad structureless emission band centered at 465 nm was observed (Fig. 2a). For **NI-Py**, a broad, structureless emission band centered at 500 nm was observed, which is assigned to the NI moiety in the dyad. Note this is an interesting example of Förster resonance energy transfer (FRET) that the fluorescence emission of the energy donor (NI) overlap with the absorption spectrum of the energy acceptor unit (Perylene) in nonpolar solvents (see ESI, Fig. S18), but most of the emission spectrum is on the red-side of the absorption spectrum of the energy acceptor [71]. Previously, we observed a similar phenomenon with a FRET pairs based on Bodipy derivatives [72]. In these cases, the Stokes shifts of the energy donor and acceptors play a role for the observation, and the comparison of the relaxed S_1 states of the energy donor and acceptor may rationalize the unusual FRET [73, 74]. In dichloromethane, the fluorescence emission intensity of **Py-Ph**, **NI** and **NI-Br** are similar, but the emission of **NI-Py** became much weaker, and the emission band (FWHM: 4230 cm^{-1}) is much broader than the **NI** and **NI-Br** (FWHM: 2900 cm^{-1}). Therefore, we propose that the emissive state of **NI-Py** in DCM is drastically different from that of **NI/NI-Br**.

We propose the emissive state is a CT state with NI as an electron acceptor and perylene unit as electron donor, it is different from the intramolecular charge transfer (ICT) state of **NI** and **NI-Br**. The quenched emission of **NI-Py** is more significant in ACN (Fig. 2c). The different emissive state of **NI-Py** as compared to **NI** and **NI-Br**, especially in polar

solvents, is supported by the analysis of the dipole moments of the emissive states (see later section).

To further prove that the luminescence bands of **NI-Py** are generated by the electronic interaction between D/A in the dyad, the luminescence spectra of the compounds in different solvents were studied (Fig. 3). As the polarity of the solvent increases, the emission of **NI** and **NI-Br** are only slightly red-shifted, the quenching of the fluorescence emission is not significant (Fig. 3a, b). The emission of **Py-Ph** is almost independent of the solvent polarity (Fig. 3d). On the contrary, **NI-Py** shows much red-shifted and weaker emission bands in polar solvents as compared to that in non-polar solvents, indicating the emissive state of **NI-Py** is different from the other compounds discussed herein. The emission

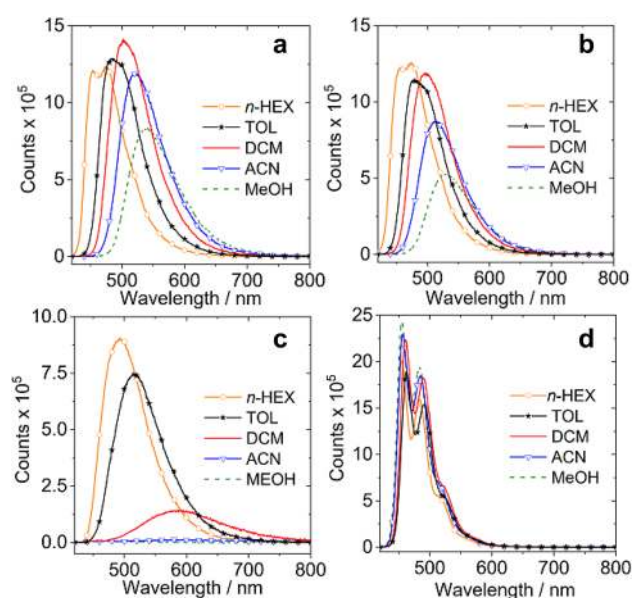


Fig. 3 Fluorescence emission spectra of **a** **NI** **b** **NI-Br** **c** **NI-Py** and **d** **Py-Ph** in different solvents. Optically matched solutions were used ($A=0.242$ at 410 nm), $20\text{ }^{\circ}\text{C}$

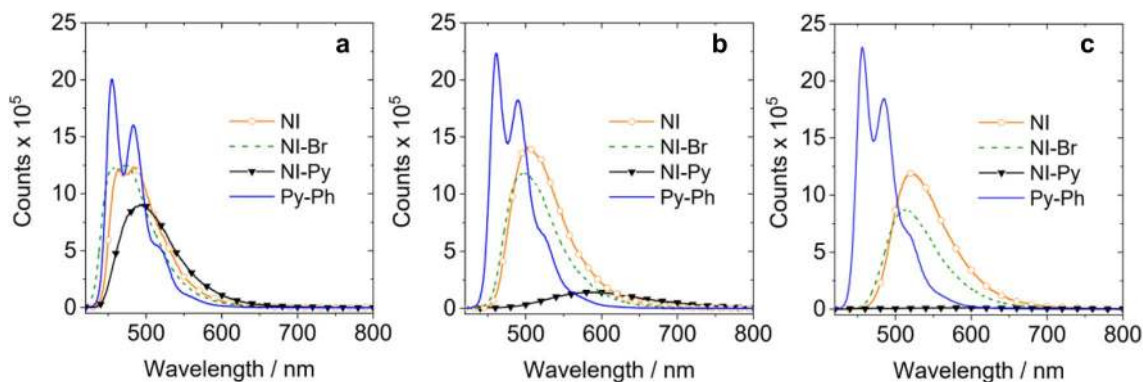


Fig. 2 Fluorescence emission spectra of **NI**, **NI-Br**, **NI-Py** and **Py-Ph** in **a** hexane, **b** dichloromethane, **c** acetonitrile. Optically matched solutions were used ($A=0.242$ at 410 nm), $c = \text{ca. } 1.0 \times 10^{-5}\text{ M}$, $20\text{ }^{\circ}\text{C}$

Table 1 Photophysical properties of the compounds

	λ_{abs} (nm) ^a	ϵ ^b	λ_{em} (nm) ^a	τ_{F} (ns) ^c	Φ_{F} (%) ^d	τ_{T} (μs) ^e	k_{r} (10^7s^{-1}) ^f	k_{nr} (10^7s^{-1}) ^g
NI-Py	421/447	0.4/0.5	584	7.6	15.2	175	2.0	11.2
Py-Ph	420/446	0.3/0.4	461	3.8 (98%) 25.3 (2%)	91.0	— ^h	21.5	2.1
NI	426	0.2	501	10.6	91.8	— ^h	8.7	0.77
NI-Br	412	0.2	494	7.7	99.7	16	12.9	0.04

^aIn DCM, $c = 1.0 \times 10^{-5}$ M^bMolar absorption coefficient ϵ , in $10^5 \text{M}^{-1} \text{cm}^{-1}$ ^cFluorescence quantum yield in ns^dAbsolute fluorescence quantum yield^eThe triplet state lifetime, in μs ^fRadiative rate constant of the CT emission band^gNonradiative rate constant of the CT emission band^hNot observed**Table 2** Fluorescence quantum yields (Φ_{F}) of the compounds in different solvents^a

Compounds ^b	HEX	TOL	DCM	ACN	MEOH
NI-Py	57.6%	61.9%	15.2%	1.6%	0.2%
NI-Br	66.6%	72.8%	69.7%	55.9%	35.1%
Py-Ph	68.5%	84.2%	91.0%	80.4%	80.0%
NI	70.1%	82.8%	91.8%	79.2%	60.9%

^aThe E_{T} (30) values of the solvents in kcal/mol are HEX (31.0), TOL (33.9), DCM (40.7) and ACN (45.6)^bAbsolute fluorescence quantum yield (Φ_{F}) of compounds

is assigned to be from a CT state with NI moiety as electron acceptor and perylene unit as electron donor. Similar CT emission was observed for compact electron donor/acceptor dyads [17, 42, 43, 46, 53, 75, 76].

The photophysical properties of the compounds are summarized in Table 1. The fluorescence quantum yield of **NI-Py** (15.2% in DCM) is much lower than the other compounds (Tables 1 and 2). The non-radiative decay rate constant of the emissive S_1 state of **NI-Py** is much larger than the other compounds indicates the efficient non-radiative decay channel for this compound. The fluorescence quantum yield of **NI-Py** in DCM (15.2) is higher than the recently reported NI-*perylene* analogue without the amino substituent (5.6%) [52].

Thus, we propose the electron transfer of **NI-Py** is less efficient than the recently reported analogue [52]. The solvent-dependent fluorescence of the compounds was studied in detail (Table 2). **NI-Py** is highly fluorescent in low-polarity solvent, for instance, in toluene, $\Phi_{\text{F}} = 61.9\%$. As the polarity of the solvent increases, the luminescence quantum yield gradually decreases. In a highly polar solvent (MeOH), the fluorescence is almost completely quenched. This is consistent with the **NI-Py** emission

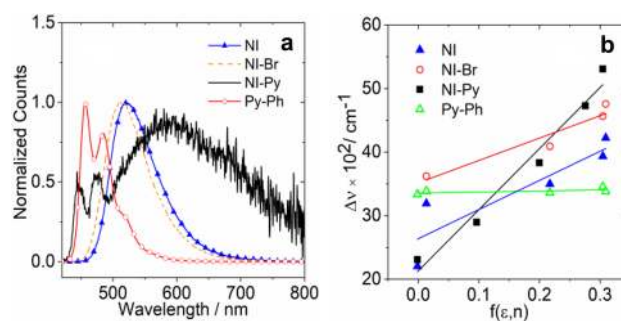


Fig. 4 **a** Normalized fluorescence emission spectra of **NI**, **NI-Br**, **NI-Py** and **Py-Ph** in acetonitrile. **b** Linear fitting of Lippert–Mataga model based on the solvatochromic shift of the energy related to the fluorescence maxima in different solvents

spectra. The absolute fluorescence quantum yield of **NI-Br** decreases with increasing solvent polarity to much less extent (Table 2). The absolute fluorescence quantum yields of **Py-Ph** and **NI** do not change significantly with increasing solvent polarity. The normalized emission spectrum in acetonitrile shows that the compound **NI-Py** has a fine-structured luminescence peak at about 450–500 nm (Fig. 4a), which is assigned to the LE-state emission of the perylene unit, and a broad structureless emission band centred at 600 nm was also observed, which is attributed to the emission of charge transfer state. This state is different from the ICT featured emissive state of the compounds **NI** and **NI-Br**, for which the emission bands are at much shorter wavelength. Based on the solvent polarity-dependent fluorescence emission data, the Lippert–Mataga plots of the compounds are constructed to derive the dipole moments of the emissive excited states of the compounds (Fig. 4b) [65, 71].

The regression is based on the Lippert–Mataga equation:

Table 3 The dipole moment of the states of the compounds. μ_g and μ_e represent the dipole moment of the ground state, singlet excited state by experiment results

Compounds	$\mu_g(\text{D})^a$	$\mu_e(\text{D})^b$
NI-Py	7.16 (S_0)	19.92 (^1CT)
NI-Br	0.23 (S_0)	2.03 (^1LE)
Py-Ph	7.88 (S_0)	17.15 (^1LE)
NI	5.83 (S_0)	11.72 (^1LE)

^aThe dipole moment of ground states of the compounds, calculated by the DFT//B3LYP/6-31G(d)

^bThe dipole moment of singlet excited states of the compounds, obtained by Lippert–Mataga plot

$$hc\left(\bar{\nu}_{\text{abs}}^{\text{CT}} - \bar{\nu}_{\text{flu}}^{\text{CT}}\right) = hc\left(\bar{\nu}_{\text{abs}}^{\text{vac}} - \bar{\nu}_{\text{flu}}^{\text{vac}}\right) + \frac{2(\bar{\mu}_e - \bar{\mu}_g)^2}{a_0^3} \left[\frac{\epsilon - 1}{2\epsilon + 1} - \frac{n^2 - 1}{2n^2 + 1} \right] \quad (2)$$

$$hc\left(\bar{\nu}_{\text{abs}}^{\text{CT}} - \bar{\nu}_{\text{flu}}^{\text{CT}}\right) = hc\left(\nu_a - \nu_f\right) = hc\left(\nu_a^0 - \nu_f^0\right) \frac{2(\bar{\mu}_e - \bar{\mu}_g)^2}{a^3} f(\epsilon, n) \quad (3)$$

μ_e is the excited state dipole moment, μ_g is the ground-state dipole moment, a is the solvent Onsager cavity radius, ϵ

is the solvent dielectric and n is the solvent refractive index, $(\nu_a - \nu_f)$ is the Stokes-shift [71, 77]. The dipole moment of the excited state of the compound can be calculated from the Lippert–Mataga formula. The ground state dipole moment (Table 3) of the compound is obtained from the calculation, thereby obtaining the excited state dipole moment. It can be seen the slope of **NI–Py** is the largest, and the calculated difference between the dipole distance between the excited state and the ground state is 12.76 D. The Lippert–Mataga plots indicate that the dipole moment of the emissive singlet excited state of **NI–Py** is 19.92 D.

The UV–Vis absorption and fluorescence excitation spectra of **NI–Py** in different solvents were compared (Fig. 5) to study the energy transfer and electron transfer in the dyad. The excitation and absorption spectra of **NI–Py** in different solvents are similar, indicating that the energy transfer or the charge separation by photoexcitation into the two parts are with the same efficiency (Fig. 5).

Fluorescence lifetime was used in different solutions (Fig. 6). The fluorescence lifetime of **NI–Py** in DCM is 7.6 ns, which is similar to that of **NI–Br** (7.7 ns) and **NI** (11.8 ns). In ACN solution, however, the fluorescence decay of **NI–Py** is with a double exponential fit (at 588 nm), which

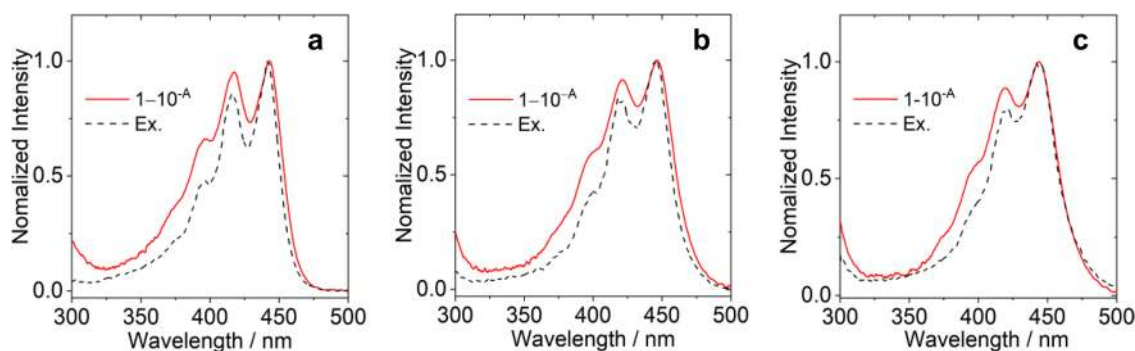


Fig. 5 Normalized fluorescence excitation spectra and UV–Vis absorption spectra of **NI–Py** in **a** *n*-hexane, $\lambda_{\text{em}} = 550$ nm; **b** dichloromethane, $\lambda_{\text{em}} = 650$ nm and **c** acetonitrile, $\lambda_{\text{em}} = 650$ nm, $c = 1.0 \times 10^{-5}$ M, 20 °C

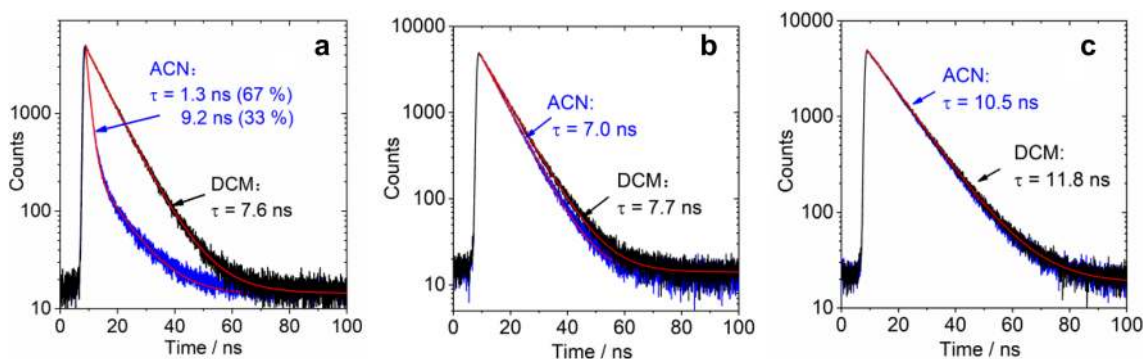


Fig. 6 Fluorescence lifetime decay traces of **a** **NI–Py** at 562 nm in dichloromethane, and 588 nm in acetonitrile; **b** **NI–Br** at 489 nm in dichloromethane, and 518 nm in acetonitrile; **c** **NI** at 492 nm in dichloromethane, and 526 nm in acetonitrile. $\lambda_{\text{ex}} = 405$ nm, $c = 1.0 \times 10^{-5}$ M, 20 °C

indicates that two processes exist, one with a short lifetime of 1.3 ns (population: 67%), the other with a long-life path attenuation of 9.2 ns (population: 33%). The shorter lifetime component shows the non-radiative transition of the emissive state of **NI-Py** in polar solvent.

On the contrary, the luminescence decay trace of **NI-Br** in ACN is with a single exponential fitting, the lifetime (7.0 ns) is similar to that in DCM, and the change is not obvious. **NI** shows similar fluorescence lifetimes in DCM (11.8 ns) and ACN (10.5 ns). The fluorescence lifetime of **NI-Py** in DCM (7.6 ns) is longer than a recently reported naphthalimide–perylene dyad (4.0 ns), may also contribute to the poor ISC efficiency of the **NI-Py** (see later section).

We determined the singlet oxygen ($^1\text{O}_2$) quantum yield (Φ_Δ) by a relative method (see [Experimental section](#)). The singlet oxygen quantum yields of **NI-Py** in DCM is 9.5% and 2.2% in *n*-hexane (Table 4). The formation of the triplet state depends on the polarity of the solvent, which is typical SOCT-ISC feature. The low singlet oxygen quantum yield is tentatively attributed to the mutual orientation of the NI and the perylene moieties, previously with anthryl-Bodipy compact electron donor/acceptor dyads, we show that although some dyads are with orthogonal geometry, but the mutual orientation of the electron donor and acceptor

Table 4 Singlet oxygen quantum yields (Φ_Δ) of the compounds in different solvents^a

Compounds ^b	HEX	TOL	DCM	ACN	MEOH
NI-Py	2.2%	2.6%	9.5%	— ^c	— ^c
NI-Br	16.2%	7.5%	6.6%	34.7%	^c
Py-Ph	— ^c	— ^c	— ^c	— ^c	— ^c
NI	— ^c	— ^c	— ^c	— ^c	— ^c

^aThe E_T (30) values of the solvents in kcal/mol are HEX (31.0), TOL (33.9), DCM (40.7) and ACN (45.6)

^bSinglet oxygen quantum yield (Φ_Δ) with Ru(bpy)₃[PF₆]₂ as standard ($\Phi_\Delta = 0.57$ in DCM) in different solvents

^cNot observed

plays a significant role in determination of the singlet oxygen quantum yields of the dyads [17, 43, 76].

The highest singlet oxygen quantum yield of **NI-Br** in ACN is 34.7%, in other solvents, the singlet oxygen quantum yield is low. This is an interesting result that attaching a heavy atom, at least bromine, to the chromophore does not always induce efficient ISC. We observed similar effect with naphthalimide chromophore [78]. No singlet oxygen production was detected for **NI** and **Py-Ph**, indicating the ISC is non-efficient, which is supported by the high fluorescence quantum yields (Table 1).

3.4 Femtosecond transient absorption (fs-TA) spectroscopy

To study the excited state dynamics of the dyad, the femtosecond transient absorption (fs-TA) spectra of **NI-Py** were measured in different solvents (Figs. 7 and 8). The fs-TA spectra were acquired in *n*-hexane and DCM solvents for dyad **NI-Py** and the data were analyzed using singular value decomposition and global fitting (sequential model) to obtain the species associated difference spectra (SADS).

First, the fs TA spectra of **NI-Py** in *n*-hexane were studied (Fig. 7a). Steady-state fluorescence study shows that the dyad is highly fluorescent in hexane ($\Phi_F = 57.6\%$). In *n*-hexane, **NI-Py** shows a ground state bleaching peak (GSB) at 443 nm upon femtosecond laser excitation, which is in agreement with the UV–Vis absorption spectrum of the compound (Fig. 1a). A stimulated emission (SE) band was observed at 468 nm, which corresponds to the steady state fluorescence of the compound. The excited state absorption (ESA) band in the range of 600–720 nm is attributed to an $S_1 \rightarrow S_n$ absorption of the perylene (Fig. 7a) [79]. The formation of the triplet state is not significant.

By examining the decay trace of the ESA peak of the singlet excited state at 697 nm (Fig. 7c), it was found that this singlet excited state shows a rapid decay process, with a lifetime of 5.6 ps, we suppose this is due to FRET from perylene

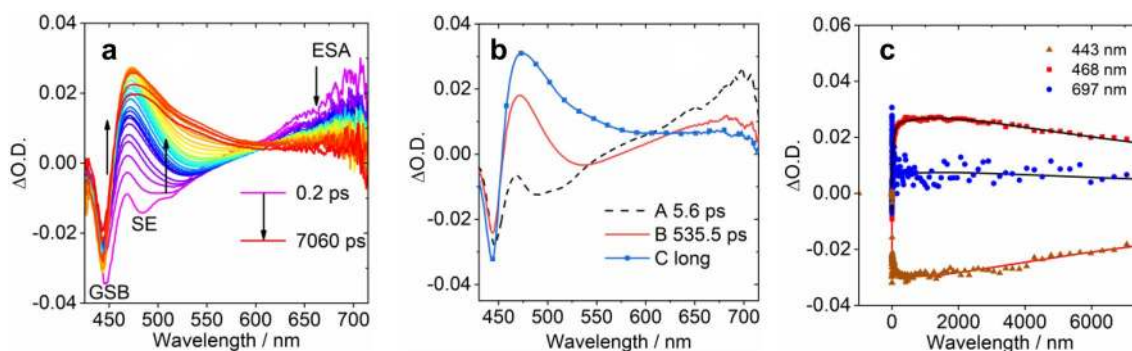


Fig. 7 **a** fs TA spectra of **NI-Py** in *n*-hexane; **b** corresponding species-associated difference spectra (SADS) obtained from global fitting and target analysis and **c** kinetic traces at selected wavelengths with their fitting lines; conditions: $\lambda_{\text{ex}} = 400$ nm, 20 °C

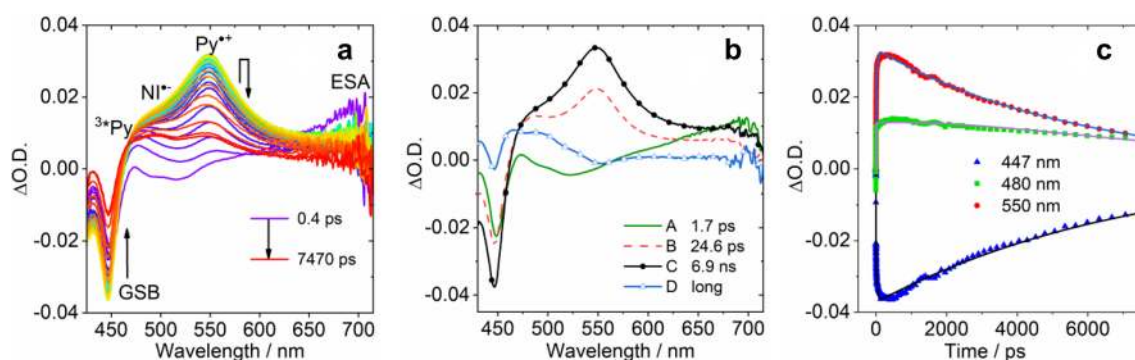


Fig. 8 **a** Femtosecond transient absorption spectra of **NI-Py** in DCM at different delay times. **b** Corresponding species-associated difference spectra (SADS) obtained from target analysis and **c** kinetic traces at selected wavelengths. $\lambda_{\text{ex}} = 400 \text{ nm}$, $20 \text{ }^\circ\text{C}$

to the NI moiety [80]. Then a broad band absorption band centered at 468 nm is resulted, which is with lifetime of 535.5 ps, which is supposed to be geometry relation and minor ISC process. The long-lived final species is in principle the S_1 state of the NI moiety. No obvious charge separation (see fs TA results in DCM) was observed in hexane.

For **NI-Py** in dichloromethane, the GSB band is centered at about 445 nm, and an ESA band at 550 nm is intensified after excitation (Fig. 8a), which is attributed to the absorption of perylene radical cation [52]. The weak absorption band at ca. 470 nm may be attributed to the absorption of the NI radical anion [42]. With global fitting, the SADS spectra were obtained (Fig. 8b). At short delay time, the ESA band centered at 720 nm (species A, the black line in Fig. 8b) is assigned to the perylene singlet excited state ($S_1 \rightarrow S_n$ transition). The lifetime of this species is 1.7 ps. Since the species B is with significant CT absorption character, thus the CS takes 1.7 ps. Species B is with lifetime of 24.6 ps, which developed to a species C which show stronger absorption band at 550 nm, which may be attributed to geometry/solvation relaxation. Species C is with lifetime of 6.9 ns, and it developed to the final long-lived state (species D, triplet state). Thus the CR-induced ISC takes ca. 6.9 ns. This time constant is similar to the fluorescence lifetime of **NI-Py** in DCM (7.6 ns). This result indicates that the triplet state is produced after charge separate and most probably via the SOCT-ISC mechanism as found with several electron donor/acceptor systems previously. [53].

3.5 Nanosecond transient absorption spectroscopy: formation of triplet state

Nanosecond transient absorption (ns-TA) spectra were used to study the triplet state of the compounds (Fig. 9a, b). In deaerated DCM, the ns-TA spectrum of **NI-Py** shows two apparent ESA bands centered at 430 nm and 480 nm, respectively. This is the typical feature of the perylene-localized triplet state. [79, 81] There is a broad, weak, ESA band in

the range of 550 nm–700 nm and no ground-state bleaching peak was detected, this is due to the overlap of the ESA band and the GSB band at 445 nm. The triplet lifetime was determined as 175 μs by monitoring the decay trace at 510 nm (intrinsic triplet state lifetime, obtained with a kinetic model with triplet–triplet annihilation quenching effect considered). The apparent triplet state lifetime is 126 μs . [60] In aerated solution, the triplet state lifetime was reduced to 0.2 μs (see ESI, Fig. S20). The triplet state lifetime is similar to that of the previously reported results with intramolecular photosensitizing method (ca. 270 μs) or with phenothiazine–perylene dyad (156–223 μs). [53] And the recently reported perylene–NI analogue without amino substituent (237 μs) [52]. The localization of the T_1 state on the perylene moiety is reasonable, because the $^3\text{Perylene}$ state (1.52 eV) is lower than the ^3NI state (2.21 eV) [82, 83].

The confinement of the T_1 state of **Py-NI** on the perylene unit is supported by the analysis of the ns TA spectra of the reference compounds. The ns-TA spectra of **NI-Br** were recorded (Fig. 9c, d). A GSB band centred at 430 nm was observed, this GSB peak is weak because it is superimposed with the triplet excited state absorption of the NI moiety. A broad ESA band in the range of 450 nm to 750 nm was observed, which is in agreement with the previous observations [55, 84]. However, it should be noted that the ESA band is different from the T_1 state of the NI moiety without the 4-amino substituent, which does not show broad ESA band in the range 450–750 nm [42, 52]. The triplet state lifetime was fitted as 17 μs by monitoring the decay trace at 600 nm (Fig. 7d). Interestingly, no formation of perylene radical cation absorption at 553 nm was observed, which is different from the recently reported NI–perylene analogue [52].

The ns TA of **Py-Br** was also studied (Fig. 9). The observed ESA bands are typical perylene LE triplet state in the range of 430–550 nm populated by heavy atom effect (bromo atom). By monitoring the decay curve of the ESA band at 465 nm, the lifetime of the triplet excited

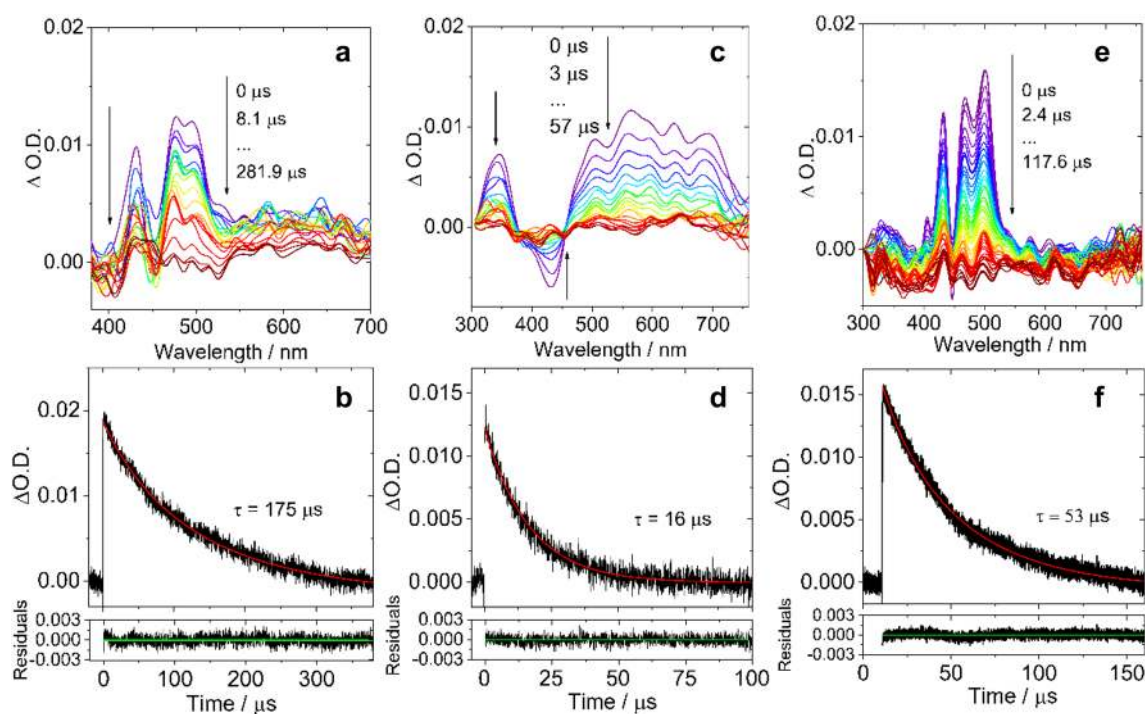


Fig. 9 Nanosecond time-resolved transient difference absorption spectroscopic studies of **a** **NI-Py** ($\lambda_{\text{ex}}=410$ nm), **c** **NI-Br** ($\lambda_{\text{ex}}=410$ nm), **e** **Py-Br** ($\lambda_{\text{ex}}=435$ nm). Decay curves of **d** **NI-Py** (at

510 nm), **d** **NI-Br** (at 600 nm), **f** **Py-Br** (at 465 nm) after pulsed laser excitation. $c = 1.0 \times 10^{-5}$ M in deaerated dichloromethane, 20 °C

state was determined as 53 μs (Fig. 9f). The comparison of the ns-TA spectra of the three compounds revealed that the triplet state of **NI-Py** is localized on the perylene unit. Moreover, it is interesting that the triplet state lifetime of **Py-Br** (53 μs), for which the triplet state is accessed with the heavy atom effect, is much shorter than that accessed with the SOCT-ISC (175 μs). Long triplet state lifetime of triplet photosensitizers is beneficial for application in phosphorescence oxygen sensing, [23, 85, 86] PDT, [87, 88] and TTA upconversion. [13, 89, 90].

The relative energy of the perylene and the NI units in the dyad **NI-Py** was also confirmed through the intermolecular triplet–triplet energy transfer (TTET) experiment. First, **NI-Br** was used as the electron donor ($E_{\text{T1}} = 2.21$ eV), [84] perylene was used as the energy acceptor ($E_{\text{T1}} = 1.52$ eV) [52]. Significant quenching of the **NI-Br** triplet state was observed (Fig. 10), with Stern–Volmer constant K_{SV} determined as $1.37 \times 10^5 \text{ M}^{-1}$. This TTET experiment indicates that the triplet state of the perylene unit is lower than the NI unit in the dyad **NI-Py**.

On the other hand, with **Py-Br** as the energy donor and NI as the energy acceptor, no quenching of the triplet state of **Py-Br** was observed (Fig. 10). This TTET result indicates that the triplet energy level of the NI moiety is higher than the perylene, thus no energy transfer is possible.

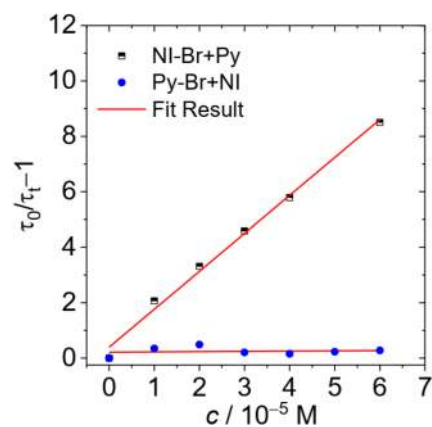


Fig. 10 Stern–Volmer plots generated from triplet state lifetime-quenching of **NI-Br** with perylene as a quencher and **Py-Br** with **NI** used as a quencher, ($\lambda_{\text{ex}}=410$ nm). c (Sensitizers) = 2.0×10^{-5} M in deaerated dichloromethane, 20 °C

3.6 DFT computations: rationalization of the photophysical properties of the compounds

DFT computations were used for study of the photophysical property of the compounds. Firstly, the ground state geometry of **NI-Py** was optimized, a dihedral angle between the

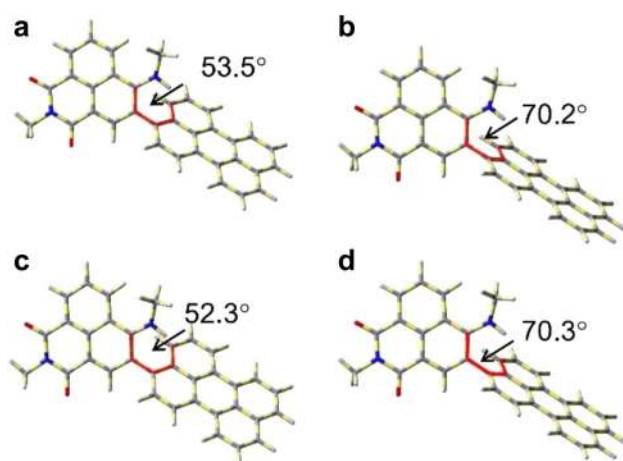
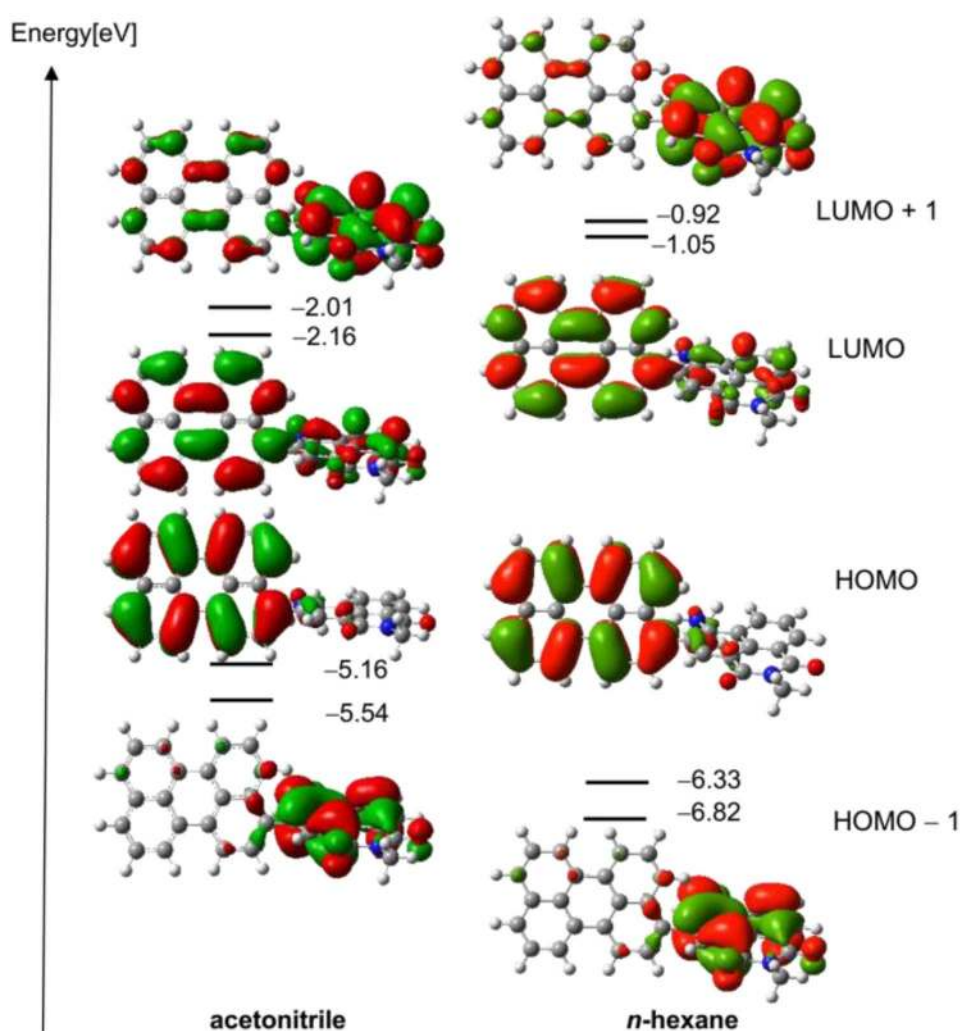


Fig. 11 Optimized molecular structures of NI-Py at **a** singlet excited state in *n*-hexane; **b** singlet excited state in acetonitrile; **c** triplet excited state in *n*-hexane and **d** triplet excited state in acetonitrile. Isovalue=0.0004 a.u.. Calculations were performed at the B3LYP/6-31G(d) level with Gaussian 09

peylene and the NI moiety of 74.2° was observed (see ESI, Fig. S25). For the singlet excited state in *n*-hexane, the dihedral angle is 53.5° (Fig. 11a). In acetonitrile, however, the dihedral angle is larger (70.2° , Fig. 11b). For the triplet state, the dihedral angle between the NI and the Py moieties is different from the S_1 state, and the T_1 state geometry is also solvent dependent.

As the solvent polarity increases, the CT state may be the lowest state. Therefore, the ground state (Fig. 12) and singlet excited state (see ESI Figs. S27 and S28†) in *n*-hexane and acetonitrile were optimized. The HOMO is mainly localized on the perylene moiety, and the LUMO is on the whole molecule. For S_1 state (2.19 eV, 567 nm. In acetonitrile), the HOMO \rightarrow LUMO is the main transition (69%), which is a CT between NI moiety and the whole molecule; thus, S_1 state is with CT character (see ESI, Table S2†). For the optimized S_2 state (2.28 eV, 545 nm, in acetonitrile), the HOMO \rightarrow LUMO + 1 is the main transition (71%), and the LUMO + 1 is delocalized on the NI moiety, which indicates charge transfer occurred from

Fig. 12 HOMO/LUMO energy levels (in eV) of NI-Py at the optimized ground state in acetonitrile and *n*-hexane (CPCM model). Calculations were performed at the B3LYP/6-31G(d) level with Gaussian 09, Isovalue=0.02 a.u.



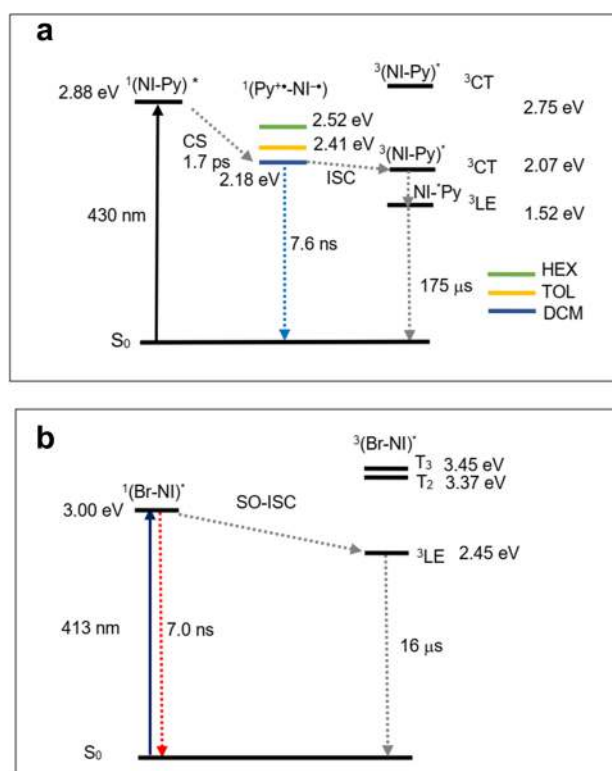
perylene to NI. The S_2 is a CT state thus may also contribute to fluorescence (see ESI Table S2†), considering the larger oscillator strength of $S_2 \rightarrow S_0$ ($f=0.711$) than that of S_1 state ($S_1 \rightarrow S_0, f=0.183$), and the similar energy of the S_2 state (2.28 eV) and the S_1 state (2.19 eV).

The triplet state was also studied with TD-DFT. For T_1 state, the molecular orbitals involved are HOMO/LUMO, which are confined on the perylene moiety, the calculated energy is 1.52 eV. For T_2 state, the molecular orbitals involved are HOMO – 1/LUMO + 1, which are more localized on the NI moiety, the state energy is 2.07 eV. These results are in agreement with the ns TA spectral data.

The spin density surfaces of the triplet state, radical anion and radical cation were computed (Fig. 13). The triplet state is localized on the perylene moiety, which is in agreement with the ns TA absorption spectra. The spin density surface of the radical anion is localized on the NI moiety, and the radical cation is confined on the perylene moiety, these results corroborate with the previous conclusion that NI unit is the electron acceptor and the perylene unit is the electron donor.

The photophysical properties of compounds are summarized in Scheme 2. For **NI-Py**, when the LE state of the molecule is excited, **NI-Py** will have a fast charge separation (1.7 ps), resulting in a CT state. Comparing the CT state energy levels in different polar solvents, it can be seen that the CT state energy levels decrease with the increase of solvent polarity, so the CT state energy levels in dichloromethane (2.18 eV) are lower than those in n-hexane (2.52 eV) and toluene (2.41 eV). The CT energy level of **NI-Py** in dichloromethane matches the T_2 energy level (2.07 eV) more closely, which proves that SOCT-ISC can occur. In the higher polarity solvents, like acetonitrile, the charge separation state energy level is lower, but no triplet state signal was observed, because the charge recombination rate in acetonitrile to the ground state is faster.

For **NI-Br**, the large energy gap between the S_1 and the T_1 states may contribute to the low ISC yield (Table 4). In acetonitrile, the energy gap is smaller, high ISC yield was observed (34.7%).



Scheme 2. The photophysical processes of **a NI-Py** and **b NI-Br** upon photoexcitation

4 Conclusions

We prepared an orthogonal compact electron donor/acceptor dyad with perylene (Py) as electron donor and 4-amino substituted naphthalimide (NI) as an electron acceptor. The perylene unit was attached at the 3-position of the NI moiety, i.e. the ortho position of the amino substituent so that steric hindrance will cause an orthogonal geometry, which is beneficial for the spin orbit charge transfer intersystem crossing (SOCT-ISC). The photophysical properties of dyad **NI-Py** were studied by steady-state UV-Vis absorption and fluorescence spectroscopies, femtosecond/nanosecond transient absorption spectroscopies and DFT computations. Ground state interaction between the NI and Py units is

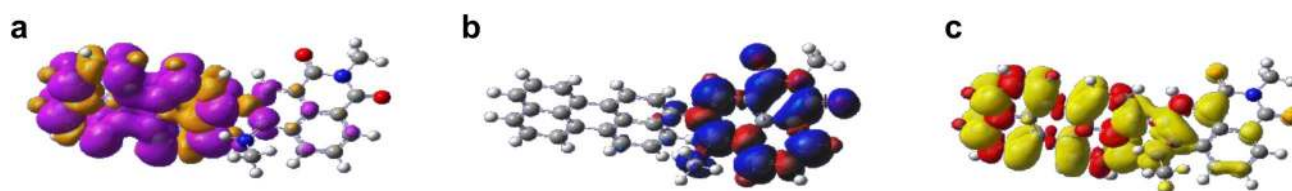


Fig. 13 Spin density distribution of the **NI-Py** **a** at triplet state of **NI-Py**; **b** radical anion $[\text{NI-Py}]^{\bullet-}$ and **c** radical cation $[\text{NI-Py}]^{\bullet+}$ in acetonitrile (CPCM model). Calculated at B3LYP/6–31G **d** level using Gaussian 09, isovalue = 0.004 a.u.

negligible; however, charge separation (CS) occurs at singlet excited-state manifold, indicated by the quenching of the fluorescence of the dyad in polar solvents, i.e. fluorescence quantum yield (Φ_F) is 61.9% in toluene and $\Phi_F = 0.2\%$ in methanol. SOCT-ISC was confirmed by femtosecond transient absorption spectroscopy, CS takes 1.7 ps and charge recombination (CR) takes 7.6 ns (in dichloromethane). These kinetics are similar to the recently reported NI-perylene analogue (0.66 ps and 8 ns, respectively). Nanosecond transient absorption spectra indicate the formation of perylene-localized triplet state, and the intrinsic triplet state lifetime (175 μ s). It is much longer than that accessed with the heavy atom effect (53 μ s, for 3-bromoperylene). The singlet oxygen quantum (Φ_Δ) yield is 2.2% in hexane and 9.5% in dichloromethane. The low SOCT-ISC efficiency ($\Phi_\Delta = 9.5\%$) as compared to the previously reported analogue ($\Phi_\Delta = 80\%$) is attributed to the mismatch of the 1 CT and the T_n states energies and the mutual orientation of the NI and the perylene units (although orthogonal is achieved in the current dyad, yet the dipole–dipole mutual orientation of the electron donor/acceptor is different from the previously reported analogue showing higher ISC efficiency. These information are useful for design of new compact electron donor/acceptor dyads as heavy atom-free triplet photosensitizers showing efficient intersystem crossing ability.

Acknowledgements X. Li thanks the NSFC (21576043) for financial support. J. Zhao thanks the NSFC (U2001222, 21673031, 21761142005 and 21911530095) and the State Key Laboratory of Fine Chemicals (ZYTS201901) for financial support.

References


- Kamkaew, A., Lim, S. H., Lee, H. B., Kiew, L. V., Chung, L. Y., & Burgess, K. (2013). Bodipy dyes in photodynamic therapy. *Chemical Society Reviews*, *42*, 77–88. <https://doi.org/10.1039/C2CS35216H>.
- Zhao, J., Wu, W., Sun, J., & Guo, S. (2013). Triplet photosensitizers: from molecular design to applications. *Chemical Society Reviews*, *42*, 5323–5351. <https://doi.org/10.1039/C3CS35531D>.
- Zhao, J., Xu, K., Yang, W., Wang, Z., & Zhong, F. (2015). The triplet excited state of bodipy: Formation, modulation and application. *Chem. Soc. Rev.*, *44*, 8904–8939. <https://doi.org/10.1039/C5CS00364D>.
- Zheng, J., Swords, W. B., Jung, H., Skubi, K. L., Kidd, J. B., Meyer, G. J., et al. (2019). Enantioselective intermolecular excited-state photoreactions using a chiral IR triplet sensitizer: separating association from energy transfer in asymmetric photocatalysis. *Journal of the American Chemical Society*, *141*, 13625–13634. <https://doi.org/10.1021/jacs.9b06244>.
- Dong, R., Chen, K.-K., Wang, P., Zhang, N., Guo, S., Zhang, Z.-M., & Lu, T.-B. (2019). Heavy atom-free keto-di-coumarin as earth-abundant strong visible light-harvesting photosensitizer for efficient photocatalytic hydrogen evolution. *Dyes. Pigments*, *166*, 84–91. <https://doi.org/10.1016/j.dyepig.2019.03.019>.
- Mahammed, A., Chen, K., Vestfrid, J., Zhao, J., & Gross, Z. (2019). Phosphorus corrole complexes: From property tuning to applications in photocatalysis and triplet–triplet annihilation upconversion. *Chem. Sci.*, *10*, 7091–7103. <https://doi.org/10.1039/C9SC01463B>.
- Agazzi, M. L., Almodovar, V. A. S., Gsponer, N. S., Bertolotti, S., Tomé, A. C., & Durantini, E. N. (2020). Diketopyrrolopyrrole–fullerene C_{60} architectures as highly efficient heavy atom-free photosensitizers: synthesis, photophysical properties and photodynamic activity. *Organic & Biomolecular Chemistry*, *18*, 1449–1461. <https://doi.org/10.1039/C9OB02487E>.
- Wang, Z., Ivanov, M., Gao, Y., Bussotti, L., Foggi, P., Zhang, H., et al. (2020). Spin–orbit charge-transfer intersystem crossing (ISC) in compact electron donor–acceptor dyads: ISC mechanism and application as novel and potent photodynamic therapy reagents. *Chemistry—A European Journal*, *26*, 1091–1102. <https://doi.org/10.1002/chem.201904306>.
- Qian, M., Hou, W., Chen, D., Li, X., Chen, Q., & Wu, C. (2019). Metalloporphyrin loaded semiconducting polymer dots as potent photosensitizers via triplet–triplet energy transfer. *J. Photochem. Photobio*, *383*, 111988. <https://doi.org/10.1016/j.jphotochem.2019.111988>.
- Majumdar, P., Nomula, R., & Zhao, J. (2014). Activatable triplet photosensitizers: magic bullets for targeted photodynamic therapy. *J. Mater. Chem. C*, *2*, 5982–5997. <https://doi.org/10.1039/C4TC00659C>.
- Wong, W. Y., & Ho, C. L. (2006). Di-, oligo- and polymetallaynes: syntheses, photophysics, structures and applications. *Coordination Chemistry Reviews*, *250*, 2627–2690.
- Singh-Rachford, T. N., & Castellano, F. N. (2010). Photon upconversion based on sensitized triplet–triplet annihilation. *Coordination Chemistry Reviews*, *254*, 2560–2573. <https://doi.org/10.1016/j.ccr.2010.01.003>.
- Zhao, J., Ji, S., & Guo, H. (2011). Triplet–triplet annihilation based upconversion: From triplet sensitizers and triplet acceptors to upconversion quantum yields. *RSC Adv.*, *1*, 937–950. <https://doi.org/10.1039/C1RA00469G>.
- Zhou, J., Liu, Q., Feng, W., Sun, Y., & Li, F. (2015). Upconversion luminescent materials: Advances and applications. *Chemical Reviews*, *115*, 395–465. <https://doi.org/10.1021/cr400478f>.
- Lv, W., Li, Y., Li, F., Lan, X., Zhang, Y., Du, L., et al. (2019). Upconversion-like photolysis of bodipy-based prodrugs via a one-photon process. *Journal of the American Chemical Society*, *141*, 17482–17486. <https://doi.org/10.1021/jacs.9b09034>.
- Tanaka, K., Ohashi, W., Inafuku, K., Shiotsu, S., & Chujo, Y. (2020). Development of the sensitizer for generating higher-energy photons under diluted condition via the triplet–triplet annihilation-supported upconversion. *Dyes. Pigments*, *172*, 107821. <https://doi.org/10.1016/j.dyepig.2019.107821>.
- Wang, Z., & Zhao, J. (2017). Bodipy–anthracene dyads as triplet photosensitizers: effect of chromophore orientation on triplet-state formation efficiency and application in triplet–triplet annihilation upconversion. *Organic Letters*, *19*, 4492–4495. <https://doi.org/10.1021/acs.orglett.7b02047>.
- Ye, C., Zhou, L., Wang, X., & Liang, Z. (2016). Photon upconversion: From two-photon absorption (TPA) to triplet–triplet annihilation (TTA). *Physical Chemistry Chemical Physics*, *18*, 10818–10835. <https://doi.org/10.1039/C5CP07296D>.
- Prieto-Montero, R., Sola-Llano, R., Montero, R., Longarte, A., Arbeloa, T., López-Arbeloa, I., et al. (2019). Methylthio bodipy as a standard triplet photosensitizer for singlet oxygen production: a photophysical study. *Physical Chemistry Chemical Physics*, *21*, 20403–20414. <https://doi.org/10.1039/C9CP03454D>.
- 20Y. Wei, Y. Li, M. Zheng, X. Zhou, Y. Zou and C. Yang, Simultaneously high upconversion efficiency and large anti-stokes shift by using Os(II) complex dyad as triplet photosensitizer, *Adv. Opt. Mater.*, 2020, **8**, 1902157. DOI:<https://doi.org/10.1002/adom.201902157>

21. Islangulov, R. R., Lott, J., Weder, C., & Castellano, F. N. (2007). Noncoherent low-power upconversion in solid polymer films. *Journal of the American Chemical Society*, *129*, 12652–12653. <https://doi.org/10.1021/ja075014k>.
22. Mahmood, Z., Taddei, M., Rehmat, N., Bussotti, L., Doria, S., Guan, Q., et al. (2020). Color-tunable delayed fluorescence and efficient spin–orbit charge transfer intersystem crossing in compact carbazole–anthracene–bodipy triads employing the sequential electron transfer approach. *Journal of Physical Chemistry C*, *124*, 5944–5957. <https://doi.org/10.1021/acs.jpcc.9b11687>.
23. Feng, Y., Cheng, J., Zhou, L., Zhou, X., & Xiang, H. (2012). Ratiometric optical oxygen sensing: a review in respect of material design. *Analyst*, *137*, 4885–4901. <https://doi.org/10.1039/C2AN35907C>.
24. You, Y., & Nam, W. (2012). Photofunctional triplet excited states of cyclometalated Ir(III) complexes: beyond electroluminescence. *Chemical Society Reviews*, *41*, 7061–7084. <https://doi.org/10.1039/C2CS35171D>.
25. L. Flamigni, A. Barbieri, C. Sabatini, B. Ventura and F. Barigelletti, in *Photochemistry and photophysics of coordination compounds*, eds. V. Balzani and S. Campagna, Springer Berlin Heidelberg, Berlin, Heidelberg, 2007, pp. 143–203.
26. J. A. G. Williams, in *Photochemistry and photophysics of coordination compounds II*, eds. V. Balzani and S. Campagna, Springer Berlin Heidelberg, Berlin, Heidelberg, 2007, pp. 205–268.
27. Sun, J., Zhong, F., Yi, X., & Zhao, J. (2013). Efficient enhancement of the visible-light absorption of cyclometalated Ir(III) complexes triplet photosensitizers with bodipy and applications in photooxidation and triplet–triplet annihilation upconversion. *Inorganic Chemistry*, *52*, 6299–6310. <https://doi.org/10.1021/ic302210b>.
28. Che, Y., Yuan, X., Cai, F., Zhao, J., Zhao, X., Xu, H., & Liu, L. (2019). Bodipy–corrole dyad with truxene bridge: Photophysical properties and application in triplet–triplet annihilation upconversion. *Dyes. Pigments*, *171*, 107756. <https://doi.org/10.1016/j.dyepig.2019.107756>.
29. Lu, Y., Conway-Kenny, R., Twamley, B., McGoldrick, N., Zhao, J., & Draper, S. M. (2017). 1,10-phenanthroline ruthenium(II) complexes as model systems in the search for high-performing triplet photosensitizers: Addressing ligand versus metal effects. *ChemPhotoChem*, *1*, 544–552. <https://doi.org/10.1002/cptc.201700158>.
30. Cui, X., Zhao, J., Mohmood, Z., & Zhang, C. (2016). Accessing the long-lived triplet excited states in transition-metal complexes: Molecular design rationales and applications. *Chemical Record*, *16*, 173–188. <https://doi.org/10.1002/tcr.201500237>.
31. Nguyen, V.-N., Qi, S., Kim, S., Kwon, N., Kim, G., Yim, Y., et al. (2019). An emerging molecular design approach to heavy-atom-free photosensitizers for enhanced photodynamic therapy under hypoxia. *Journal of the American Chemical Society*, *141*, 16243–16248. <https://doi.org/10.1021/jacs.9b09220>.
32. Li, X., Kolemen, S., Yoon, J., & Akkaya, E. U. (2017). Activatable photosensitizers: agents for selective photodynamic therapy. *Advanced Functional Materials*, *27*, 1604053. <https://doi.org/10.1002/adfm.201604053>.
33. Wang, J., Hou, Y., Lei, W., Zhou, Q., Li, C., Zhang, B., & Wang, X. (2012). DNA photocleavage by a cationic bodipy dye through both singlet oxygen and hydroxyl radical: New insight into the photodynamic mechanism of bodipys. *ChemPhysChem*, *13*, 2739–2747. <https://doi.org/10.1002/cphc.201200224>.
34. Verhoeven, J. (2006). On the role of spin correlation in the formation, decay, and detection of long-lived, intramolecular charge-transfer states. *Journal of Photochemistry and Photobiology C*, *7*, 40–60. <https://doi.org/10.1016/j.jphotochem.2006.04.001>.
35. Vauthey, E. (2012). Photoinduced symmetry-breaking charge separation. *ChemPhysChem*, *13*, 2001–2011. <https://doi.org/10.1002/cphc.201200106>.
36. Verhoeven, J. W., van Ramesdonk, H. J., Groeneveld, M. M., Beniston, A. C., & Harriman, A. (2005). Long-lived charge-transfer states in compact donor–acceptor dyads. *Chem Phys Chem*, *6*, 2251–2260. <https://doi.org/10.1002/cphc.200500029>.
37. Gibbons, D. J., Farawar, A., Mazzella, P., Leroy-Lhez, S., & Williams, R. M. (2020). Making triplets from photo-generated charges: observations, mechanisms and theory. *Photochemical & Photobiological Sciences*, *19*, 136–158. <https://doi.org/10.1039/C9PP00399A>.
38. Filatov, M. A. (2020). Heavy-atom-free bodipy photosensitizers with intersystem crossing mediated by intramolecular photoinduced electron transfer. *Organic & Biomolecular Chemistry*, *18*, 10–27. <https://doi.org/10.1039/C9OB02170A>.
39. Hou, Y., Zhang, X., Chen, K., Liu, D., Wang, Z., Liu, Q., et al. (2019). Charge separation, charge recombination, long-lived charge transfer state formation and intersystem crossing in organic electron donor/acceptor dyads. *J. Mater. Chem. C*, *7*, 12048–12074. <https://doi.org/10.1039/C9TC04285G>.
40. Kc, C. B., Lim, G. N., Nesterov, V. N., Karr, P. A., & D’Souza, F. (2014). Phenothiazine–bodipy–fullerene triads as photosynthetic reaction center models: Substitution and solvent polarity effects on photoinduced charge separation and recombination. *Chemistry—A European Journal*, *20*, 17100–17112. <https://doi.org/10.1002/chem.201404863>.
41. X.-F. Zhang and N. Feng, Attaching naphthalene derivatives onto bodipy for generating excited triplet state and singlet oxygen: tuning pet-based photosensitizer by electron donors, *Spectrochim. Acta Part A: Mol. and Biomol. Spectro.*, 2018, **189**, 13–21. DOI:<https://doi.org/10.1016/j.saa.2017.08.005>
42. Tang, G., Sukhanov, A. A., Zhao, J., Yang, W., Wang, Z., Liu, Q., et al. (2019). Red thermally activated delayed fluorescence and the intersystem crossing mechanisms in compact naphthalimide–phenothiazine electron donor/acceptor dyads. *Journal of Physical Chemistry C*, *123*, 30171–30186. <https://doi.org/10.1021/acs.jpcc.9b09335>.
43. Wang, Z., Sukhanov, A. A., Toffoletti, A., Sadiq, F., Zhao, J., Barbon, A., et al. (2019). Insights into the efficient intersystem crossing of bodipy–anthracene compact dyads with steady-state and time-resolved optical/magnetic spectroscopies and observation of the delayed fluorescence. *Journal of Physical Chemistry C*, *123*, 265–274. <https://doi.org/10.1021/acs.jpcc.8b10835>.
44. Dance, Z. E. X., Mi, Q., McCamant, D. W., Ahrens, M. J., Ratner, M. A., & Wasielewski, M. R. (2006). Time-resolved EPR studies of photogenerated radical ion pairs separated by *p*-phenylene oligomers and of triplet states resulting from charge recombination. *The Journal of Physical Chemistry B*, *110*, 25163–25173. <https://doi.org/10.1021/jp063690n>.
45. Dance, Z. E. X., Mickle, S. M., Wilson, T. M., Ricks, A. B., Scott, A. M., Ratner, M. A., & Wasielewski, M. R. (2008). Intersystem crossing mediated by photoinduced intramolecular charge transfer: Julolidine–anthracene molecules with perpendicular π systems. *Journal of Physical Chemistry A*, *112*, 4194–4201. <https://doi.org/10.1021/jp800561g>.
46. Filatov, M. A., Karuthedath, S., Polestshuk, P. M., Savoie, H., Flanagan, K. J., Sy, C., et al. (2017). Generation of triplet excited states via photoinduced electron transfer in meso-anthra-bodipy: Fluorogenic response toward singlet oxygen in solution and in vitro. *Journal of the American Chemical Society*, *139*, 6282–6285. <https://doi.org/10.1021/jacs.7b00551>.
47. Hou, Y., Biskup, T., Rein, S., Wang, Z., Bussotti, L., Russo, N., et al. (2018). Spin–orbit charge recombination intersystem crossing in phenothiazine–anthracene compact dyads: effect of molecular conformation on electronic coupling, electronic

- transitions, and electron spin polarizations of the triplet states. *Journal of Physical Chemistry C*, *122*, 27850–27865. <https://doi.org/10.1021/acs.jpcc.8b08965>.
48. Callaghan, S., Filatov, M. A., Savoie, H., Boyle, R. W., & Senge, M. O. (2019). In vitro cytotoxicity of a library of bodipy-anthracene and -pyrene dyads for application in photodynamic therapy. *Photochemical & Photobiological Sciences*, *18*, 495–504. <https://doi.org/10.1039/C8PP00402A>.
49. Hu, W., Liu, M., Zhang, X.-F., Wang, Y., Wang, Y., Lan, H., & Zhao, H. (2019). Can bodipy-electron acceptor conjugates act as heavy atom-free excited triplet state and singlet oxygen photosensitizers via photoinduced charge separation-charge recombination mechanism? *Journal of Physical Chemistry C*, *123*, 15944–15955. <https://doi.org/10.1021/acs.jpcc.9b02961>.
50. Chen, K., Yang, W., Wang, Z., Iagatti, A., Bussotti, L., Foggi, P., et al. (2017). Triplet excited state of bodipy accessed by charge recombination and its application in triplet-triplet annihilation upconversion. *Journal of Physical Chemistry A*, *121*, 7550–7564. <https://doi.org/10.1021/acs.jpca.7b07623>.
51. Rehmat, N., Toffoletti, A., Mahmood, Z., Zhang, X., Zhao, J., & Barbon, A. (2020). Carbazole-erylenebisimide electron donor/acceptor dyads showing efficient spin orbit charge transfer intersystem crossing (SOCT-ISC) and photo-driven intermolecular electron transfer. *J. Mater. Chem. C*, *8*, 4701–4712. <https://doi.org/10.1039/C9TC06429J>.
52. Imran, M., El-Zohry, A. M., Matt, C., Taddei, M., Doria, S., Bussotti, L., et al. (2020). Intersystem crossing via charge recombination in a perylene-naphthalimide compact electron donor/acceptor dyad. *J. Mater. Chem. C*, *8*, 8305–8319. <https://doi.org/10.1039/D0TC00017E>.
53. Imran, M., Sukhanov, A. A., Wang, Z., Karatay, A., Zhao, J., Mahmood, Z., et al. (2019). Electronic coupling and spin-orbit charge-transfer intersystem crossing in phenothiazine-erylene compact electron donor/acceptor dyads. *Journal of Physical Chemistry C*, *123*, 7010–7024. <https://doi.org/10.1021/acs.jpcc.8b12040>.
54. 54P. de Echegaray, M. J. Mancheño, I. Arrechea-Marcos, R. Juárez, G. López-Espejo, J. T. López Navarrete, M. M. Ramos, C. Seoane, R. P. Ortiz and J. L. Segura, Synthesis of perylene imide diones as platforms for the development of pyrazine based organic semiconductors, *J. Org. Chem.*, 2016, **81**, 11256–11267. DOI:<https://doi.org/10.1021/acs.joc.6b02214>
55. Liu, L., Zhang, C., & Zhao, J. (2014). The effect of the regioisomeric naphthalimide acetylidyl ligands on the photophysical properties of N⁺N Pt(II) bisacetylidyl complexes. *Dalton Transactions*, *43*, 13434–13444. <https://doi.org/10.1039/C4DT01732C>.
56. Torres, É., Berberan-Santos, M. N., & Brites, M. J. (2015). Synthesis, photophysical and electrochemical properties of perylene dyes. *Dyes. Pigments*, *112*, 298–304. <https://doi.org/10.1016/j.dyepig.2014.07.019>.
57. Avlasevich, Y., & Müllen, K. (2007). An efficient synthesis of quaterylene-dicarboximide NIR dyes. *Journal of Organic Chemistry*, *72*, 10243–10246. <https://doi.org/10.1021/jo702019p>.
58. 58R. Fernando, Z. Mao and G. Sauvé, Rod-like oligomers incorporating 2,6-dialkylamino core-substituted naphthalene diimide as acceptors for organic photovoltaic, *Organic Electronics*, 2013, **14**, 1683–1692. DOI:<https://doi.org/10.1016/j.orgel.2013.03.039>
59. Takizawa, S.-Y., Aboshi, R., & Murata, S. (2011). Photooxidation of 1,5-dihydroxynaphthalene with iridium complexes as singlet oxygen sensitizers. *Photochemical & Photobiological Sciences*, *10*, 895–903. <https://doi.org/10.1039/C0PP00265H>.
60. Lou, Z., Hou, Y., Chen, K., Zhao, J., Ji, S., Zhong, F., et al. (2018). Different quenching effect of intramolecular rotation on the singlet and triplet excited states of bodipy. *Journal of Physical Chemistry C*, *122*, 185–193. <https://doi.org/10.1021/acs.jpcc.7b10466>.
61. Henry, E. R., & Hofrichter, J. (1992). *Method* (pp. 129–192). Enzymol.: Academic Press.
62. M. J. Frisch, G. Trucks, H. B. Schlegel, G. E. Scuseria, M. A. Robb, J. Cheeseman, G. Scalmani, V. Barone, B. Mennucci, G. A. Petersson, H. Nakatsuji, M. Caricato, X. Li, H. P. Hratchian, A. F. Izmaylov, J. Bloino, G. Zheng, J. Sonnenberg, M. Hada and D. Fox, et al., Gaussian 09 revision a.1. Gaussian inc, 2009
63. Zhao, Y., Chen, K., Yildiz, E. A., Li, S., Hou, Y., Zhang, X., et al. (2020). Efficient intersystem crossing in the tröger's base derived from 4-amino-1,8-naphthalimide and application as a potent photodynamic therapy reagent. *Chemistry—A European Journal*, *26*, 3591–3599. <https://doi.org/10.1002/chem.201905248>.
64. Filatov, M. A., Karuthedath, S., Polestshuk, P. M., Callaghan, S., Flanagan, K. J., Wiesner, T., et al. (2018). Bodipy-pyrene and perylene dyads as heavy-atom-free singlet oxygen sensitizers. *ChemPhotoChem*, *2*, 606–615. <https://doi.org/10.1002/cptc.201800020>.
65. Sasaki, S., Hattori, K., Igawa, K., & Konishi, G.-I. (2015). Directional control of π -conjugation enabled by distortion of the donor plane in diarylaminoanthracenes: a photophysical study. *Journal of Physical Chemistry A*, *119*, 4898–4906. <https://doi.org/10.1021/acs.jpca.5b03238>.
66. Shao, S., Thomas, M. B., Park, K. H., Mahaffey, Z., Kim, D., & D'Souza, F. (2018). Sequential energy transfer followed by electron transfer in a bodipy-bisstyrylbodipy bound to C₆₀ triad via a 'two-point' binding strategy. *Chemical Communications*, *54*, 54–57. <https://doi.org/10.1039/C7CC08063H>.
67. Collini, M. A., Thomas, M. B., Bandi, V., Karr, P. A., & D'Souza, F. (2017). Directly attached bisdonor-BF₂ chelated azadiopyromethene-fullerene tetrads for promoting ground and excited state charge transfer. *Chemistry—A European Journal*, *23*, 4450–4461. <https://doi.org/10.1002/chem.201700200>.
68. Wang, Z., Zhao, J., Di Donato, M., & Mazzone, G. (2019). Increasing the anti-stokes shift in TTA upconversion with photosensitizers showing red-shifted spin-allowed charge transfer absorption but a non-compromised triplet state energy level. *Chemical Communications*, *55*, 1510–1513. <https://doi.org/10.1039/C8CC08159J>.
69. Chen, K., Taddei, M., Bussotti, L., Foggi, P., Zhao, J., & Di Donato, M. (2020). Near-IR-absorbing bodipy-5,10-dihydrophenazine compact electron donor/acceptor dyads and triads: spin-orbit charge transfer intersystem crossing and charge-transfer state. *ChemPhotoChem*, *4*, 487–501. <https://doi.org/10.1002/cptc.201900294>.
70. Dong, Y., Elmali, A., Zhao, J., Dick, B., & Karatay, A. (2020). Long-lived triplet excited state accessed with spin-orbit charge transfer intersystem crossing in red light-absorbing phenoxazine-styryl bodipy electron donor/acceptor dyads. *ChemPhysChem*, *21*, 1388–1401. <https://doi.org/10.1002/cphc.202000300>.
71. Lakowicz and JosephR, *Principles of fluorescence spectroscopy*, Plenum Press, 1983.
72. Huang, L., Yang, W., & Zhao, J. (2014). Switching of the triplet excited state of styryl 2,6-diiodo-bodipy and its application in acid-activatable singlet oxygen photosensitizing. *Journal of Organic Chemistry*, *79*, 10240–10255. <https://doi.org/10.1021/jo5019014>.
73. Yu, H., Xiao, Y., Guo, H., & Qian, X. (2011). Convenient and efficient fret platform featuring a rigid biphenyl spacer between rhodamine and bodipy: transformation of 'turn-on' sensors into ratiometric ones with dual emission. *Chemistry—A European Journal*, *17*, 3179–3191. <https://doi.org/10.1002/chem.201002498>.
74. Bura, T., Nastasi, F., Puntoriero, F., Campagna, S., & Zieschel, R. (2013). Ultrafast energy transfer in triptycene-grafted bodipy scaffoldings. *Chemistry—A European Journal*, *19*, 8900–8912. <https://doi.org/10.1002/chem.201300413>.

75. Kandrashkin, Y. E., Wang, Z., Sukhanov, A. A., Hou, Y., Zhang, X., Liu, Y., et al. (2019). Balance between triplet states in photoexcited orthogonal bodipy dimers. *J. Phys. Chem. Lett.*, *10*, 4157–4163. <https://doi.org/10.1021/acs.jpcclett.9b01741>.
76. Dong, Y., Sukhanov, A. A., Zhao, J., Elmali, A., Li, X., Dick, B., et al. (2019). Spin–orbit charge-transfer intersystem crossing (SOCT-ISC) in bodipy-phenoxazine dyads: effect of chromophore orientation and conformation restriction on the photophysical properties. *Journal of Physical Chemistry C*, *123*, 22793–22811. <https://doi.org/10.1021/acs.jpcc.9b06170>.
77. Grabowski, Z. R., Rotkiewicz, K., & Rettig, W. (2003). Structural changes accompanying intramolecular electron transfer: focus on twisted intramolecular charge-transfer states and structures. *Chemical Reviews*, *103*, 3899–4032. <https://doi.org/10.1021/cr9407451>.
78. Wang, Z., Gao, Y., Hussain, M., Kundu, S., Rane, V., Hayvali, M., et al. (2018). Efficient radical-enhanced intersystem crossing in an NDI-tempo dyad: photophysics, electron spin polarization, and application in photodynamic therapy. *Chemistry—A European Journal*, *24*, 18663–18675. <https://doi.org/10.1002/chem.201804212>.
79. Xu, K., Zhao, J., & Moore, E. G. (2017). Covalently bonded perylene–diiodobodipy dyads for thiol-activatable triplet–triplet annihilation upconversion. *Journal of Physical Chemistry C*, *121*, 22665–22679. <https://doi.org/10.1021/acs.jpcc.7b06922>.
80. Pearce, N., Davies, E. S., Horvath, R., Pfeiffer, C. R., Sun, X.-Z., Lewis, W., et al. (2018). Thionated naphthalene diimides: tunable chromophores for applications in photoactive dyads. *Physical Chemistry Chemical Physics: PCCP*, *20*, 752–764. <https://doi.org/10.1039/C7CP06952A>.
81. Cui, X., El-Zohry, A. M., Wang, Z., Zhao, J., & Mohammed, O. F. (2017). Homo- or hetero-triplet–triplet annihilation? A case study with perylene-bodipy dyads/triads. *Journal of Physical Chemistry C*, *121*, 16182–16192. <https://doi.org/10.1021/acs.jpcc.7b05620>.
82. Ventura, B., Bertocco, A., Braga, D., Catalano, L., d'Agostino, S., Grepioni, F., & Taddei, P. (2014). Luminescence properties of 1,8-naphthalimide derivatives in solution, in their crystals, and in co-crystals: Toward room-temperature phosphorescence from organic materials. *Journal of Physical Chemistry C*, *118*, 18646–18658. <https://doi.org/10.1021/jp5049309>.
83. M. Montalti, A. Credi, L. Prodi and M. T. Gandolfi, Handbook of photochemistry, third edition, *Crc Press*, 2006
84. Liu, D., El-Zohry, A. M., Taddei, M., Matt, C., Bussotti, L., Wang, Z., et al. (2020). Long-lived charge-transfer state induced by Spin–orbit charge transfer intersystem crossing (SOCT-ISC) in a compact spiro electron donor/acceptor dyad. *Angewandte Chemie International Edition*, *59*, 11591–11599. <https://doi.org/10.1002/anie.202003560>.
85. Ji, S., Wu, W., Wu, W., Song, P., Han, K., Wang, Z., et al. (2010). Tuning the luminescence lifetimes of ruthenium(II) polypyridine complexes and its application in luminescent oxygen sensing. *Journal of Materials Chemistry*, *20*, 1953–1963. <https://doi.org/10.1039/B916468E>.
86. Xiang, H., Zhou, L., Feng, Y., Cheng, J., Wu, D., & Zhou, X. (2012). Tunable fluorescent/phosphorescent platinum(II) porphyrin–fluorene copolymers for ratiometric dual emissive oxygen sensing. *Inorganic Chemistry*, *51*, 5208–5212. <https://doi.org/10.1021/ic300040n>.
87. Lincoln, R., Kohler, L., Monro, S., Yin, H., Stephenson, M., Zong, R., et al. (2013). Exploitation of long-lived ³IL excited states for metal–organic photodynamic therapy: Verification in a metastatic melanoma model. *Journal of the American Chemical Society*, *135*, 17161–17175. <https://doi.org/10.1021/ja408426z>.
88. Hou, Y., Liu, Q., & Zhao, J. (2020). An exceptionally long-lived triplet state of red light-absorbing compact phenothiazine-styrylbodipy electron donor/acceptor dyads: a better alternative to the heavy atom-effect? *Chemical Communications*, *56*, 1721–1724. <https://doi.org/10.1039/C9CC09058D>.
89. Ji, S., Wu, W., Wu, W., Guo, H., & Zhao, J. (2011). Ruthenium(II) polyimine complexes with a long-lived ³IL excited state or a ³MLCT/³IL equilibrium: efficient triplet sensitizers for low-power upconversion. *Angewandte Chemie International Edition*, *50*, 1626–1629. <https://doi.org/10.1002/anie.201006192>.
90. Zhao, J., Ji, S., Wu, W., Wu, W., Guo, H., Sun, J., et al. (2012). Transition metal complexes with strong absorption of visible light and long-lived triplet excited states: From molecular design to applications. *RSC Adv.*, *2*, 1712–1728. <https://doi.org/10.1039/C1RA00665G>.

Affiliations

Xi Chen¹ · Junhong Pang² · Muhammad Imran¹ · Xiaolian Li¹ · Jianzhang Zhao^{1,3}  · Mingde Li²

¹ State Key Laboratory of Fine Chemicals, School of Chemical Engineering, Dalian University of Technology, E-208 West Campus, 2 Ling Gong Road, Dalian 116024, People's Republic of China

² Department of Chemistry and Key Laboratory for Preparation and Application of Ordered Structural Materials of Guangdong Province, Shantou University, Shantou 515063, People's Republic of China

³ School of Chemistry and Key Laboratory of Energy Materials Chemistry, Ministry of Education, Institute of Applied Chemistry, Xinjiang University, UrumqiXinjiang 830046, China